Washington University School of Medicine
Digital Commons@Becker

Open Access Publications

2018

Molecular and functional sex differences of noradrenergic neurons in the mouse locus coeruleus

Bernard Mulvey
Washington University School of Medicine in St. Louis

Dionnet L. Bhatti
Washington University School of Medicine in St. Louis

Sandeep Gyawali
Rockefeller University

Allison M. Lake
Washington University School of Medicine in St. Louis

Skrimantas Kriaucionis
University of Oxford

See next page for additional authors

Follow this and additional works at: https://digitalcommons.wustl.edu/open_access_pubs
Please let us know how this document benefits you.

Recommended Citation

Mulvey, Bernard; Bhatti, Dionnet L.; Gyawali, Sandeep; Lake, Allison M.; Kriaucionis, Skrimantas; Ford, Christopher P.; Bruchas, Michael R.; Heintz, Nathaniel; and Dougherty, Joseph D., "Molecular and functional sex differences of noradrenergic neurons in the mouse locus coeruleus." Cell reports. 23, 8. 2225-2235. (2018).
https://digitalcommons.wustl.edu/open_access_pubs/6886

This Open Access Publication is brought to you for free and open access by Digital Commons@Becker. It has been accepted for inclusion in Open Access Publications by an authorized administrator of Digital Commons@Becker. For more information, please contact vanam@wustl.edu.

Authors

Bernard Mulvey, Dionnet L. Bhatti, Sandeep Gyawali, Allison M. Lake, Skrimantas Kriaucionis, Christopher P. Ford, Michael R. Bruchas, Nathaniel Heintz, and Joseph D. Dougherty

This open access publication is available at Digital Commons@Becker: https://digitalcommons.wustl.edu/open_access_pubs/6886

Cell Reports

Molecular and Functional Sex Differences of Noradrenergic Neurons in the Mouse Locus Coeruleus

Graphical Abstract

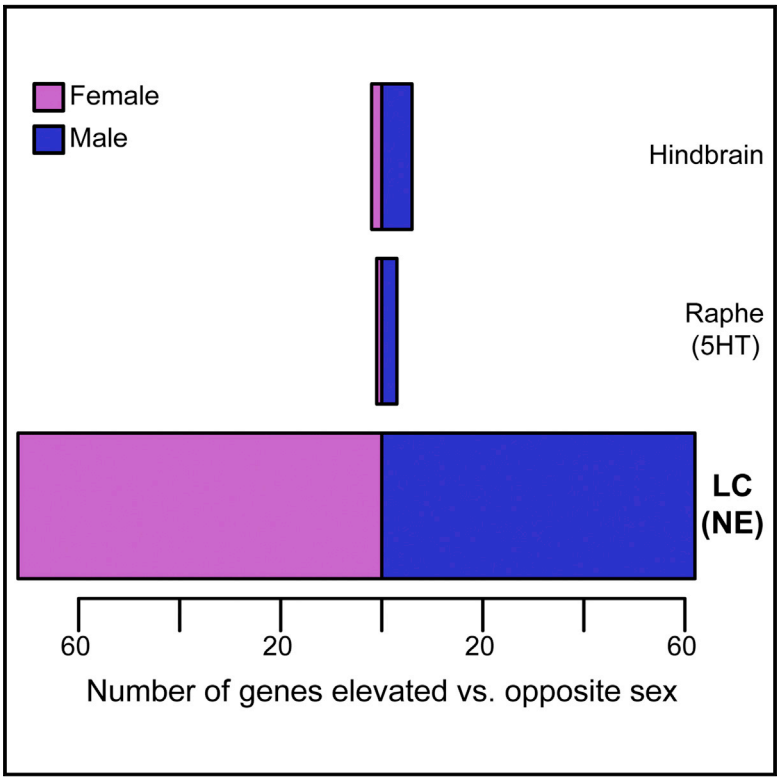

Authors

Bernard Mulvey, Dionnet L. Bhatti, Sandeep Gyawali, ..., Michael R. Bruchas, Nathaniel Heintz, Joseph D. Dougherty

Correspondence

jdougherty@genetics.wustl.edu

In Brief

Mulvey et al. present gene expression data from adult mouse norepinephrine neurons of the locus coeruleus (LC). They discover that over 100 genes are sex-differentially expressed in LC, including receptors, and that these receptor expression differences are substantial enough to have sex-specific consequences for LC neurons and the behaviors they control.

Highlights

- >3,000 genes highly expressed in adult mouse locus coeruleus (LC) are identified
- Norepinephrine neurons of LC sex-differentially express >100 genes
- PGE2 receptor *Ptger3* is more highly expressed in female LC
- PTGER3 agonism inhibits LC firing and LC-driven anxiety behavior only in female mice

Data and Software Availability

GSE100005

Mulvey et al., 2018, Cell Reports *23*, 2225–2235
May 22, 2018 © 2018 The Authors.
https://doi.org/10.1016/j.celrep.2018.04.054

CellPress

Cell Reports
Report

OPEN ACCESS
CellPress

Molecular and Functional Sex Differences of Noradrenergic Neurons in the Mouse Locus Coeruleus

Bernard Mulvey,[1] Dionnet L. Bhatti,[2] Sandeep Gyawali,[3] Allison M. Lake,[1] Skirmantas Kriaucionis,[4] Christopher P. Ford,[5] Michael R. Bruchas,[2] Nathaniel Heintz,[3] and Joseph D. Dougherty[1,6,*]
[1]Department of Genetics and Department of Psychiatry, Washington University School of Medicine, St. Louis, MO, USA
[2]Department of Anesthesiology and Department of Neuroscience, Washington University School of Medicine, St. Louis, MO, USA
[3]Laboratory of Molecular Biology, Rockefeller University, and Howard Hughes Medical Institute, New York, NY, USA
[4]Ludwig Institute for Cancer Research, University of Oxford, Oxford, UK
[5]Department of Pharmacology, University of Colorado School of Medicine, Aurora, CO, USA
[6]Lead Contact
*Correspondence: jdougherty@genetics.wustl.edu
https://doi.org/10.1016/j.celrep.2018.04.054

SUMMARY

Preclinical work has long focused on male animals, though biological sex clearly influences risk for certain diseases, including many psychiatric disorders. Such disorders are often treated by drugs targeting the CNS norepinephrine system. Despite roles for noradrenergic neurons in behavior and neuropsychiatric disease models, their molecular characterization has lagged. We profiled mouse noradrenergic neurons *in vivo*, defining over 3,000 high-confidence transcripts expressed therein, including druggable receptors. We uncovered remarkable sex differences in gene expression, including elevated expression of the EP3 receptor in females—which we leverage to illustrate the behavioral and pharmacologic relevance of these findings—and of *Slc6a15* and *Lin28b*, both major depressive disorder (MDD)-associated genes. Broadly, we present a means of transcriptionally profiling locus coeruleus under baseline and experimental conditions. Our findings underscore the need for preclinical work to include both sexes and suggest that sex differences in noradrenergic neurons may underlie behavioral differences relevant to disease.

INTRODUCTION

Numerous neuropsychiatric and neurodevelopmental diseases demonstrate a skew in incidence between sexes, including a female predominance of major depressive disorder and generalized anxiety disorder (MDD and GAD, respectively) (Kessler et al., 2005), and a male predominance of attention-deficit/hyperactivity disorder and autism spectrum disorders (ADHD and ASDs, respectively) (Christensen et al., 2016; Fombonne, 2009). Sex differences in reproductive behavior have been thoroughly attributed to sexually dimorphic brain regions; however, questions remain as to whether more modest behavioral differences—especially those relevant to common psychiatric disorders—are mediated by transcriptional sex differences in key neuronal populations.

The locus coeruleus (LC)—a small nucleus of neuromodulatory neurons whose projections release norepinephrine (NE) throughout the CNS—is implicated in a broad range of functions, including learning, novelty detection, arousal, anxiety, and fever (Sara, 2009). Given these extensive neurobehavioral roles, it is perhaps unsurprising that the LC-NE system has been broadly implicated in psychiatric disorders and animal models of them. For example, depression is often modeled in rodents using pro-inflammatory compounds including interleukins and lipopolysaccharide (LPS). LPS, besides inducing fever, is known to induce substantial activation of the LC and other noradrenergic cell types (established by Hare et al., 1995). Interleukin-6, a common upstream pro-inflammatory messenger, was recently found to directly trigger tonic firing of the LC, eliciting depressive behaviors via activation of alpha-adrenergic receptors (Kurosawa et al., 2016). Tonic firing of the LC in response to corticotropin-releasing factor (CRF) or optogenetic stimulation can also induce acute aversive and anxiety-like behaviors (McCall et al., 2015, 2017; Seo and Bruchas, 2017). Sex differences in behavioral responses to stress have been attributed to molecular-level differences in CRF signaling via the LC (Bangasser et al., 2011; Valentino and Bangasser, 2016). In the clinical setting, evidence-based practices offer a robust demonstration of the involvement of LC dysregulation—or its ability to normalize dysregulation occurring elsewhere—in psychiatric disease, given the use of NE-modulating drugs in depression, anxiety, attention-deficit/hyperactivity disorder, and addiction. Altogether, a comprehensive transcriptomic profile of the LC is of substantial interest for understanding, and potentially targeting, the molecular functions of these cells.

To date, sex differences in the rodent LC have been observed at both the single-gene and the structural level. Sex differences in stress response have been attributed to differential CRF sensitivity and CRF receptor trafficking in mouse LC (Curtis et al., 2006; Valentino et al., 2012), including sex-differential effects of CRF1 agonism on LC excitability (Bangasser et al., 2016).

This is an open access article under the CC BY license (http://creativecommons.org/licenses/by/4.0/).

μ opioid receptors are also highly expressed in the LC; μ agonism completely suppresses firing of the LC in male, but not female, mice (Guajardo et al., 2016). Reports of structural dimorphism in the rodent LC have been ambiguous, with reports of the LC being larger in either sex, depending on the strain of rat (compare Babstock et al., 1997; Bangasser et al., 2011; and Luque et al., 1992). These repeated demonstrations of sex differences in particular aspects of LC structure and function compelled us to study both sexes in our pursuit of characterizing LC gene expression.

In order to transcriptionally profile the LC, we generated a translating ribosome affinity purification (TRAP) line. We identified dozens of potential LC-specific drug targets and validated a subset of these with independent methods. We identified differentially expressed genes (DEGs) in the LC following LPS stimulation, demonstrating the utility of this line and method to detect pharmacologically mediated changes in gene expression in the LC. To our surprise, we discovered a comparable number of DEGs between sexes as well. In order to demonstrate that these transcript-level sex differences in the LC correspond to consequent physiologic differences, we modulated a receptor upregulated in female LC, EP3 (encoded by *Ptger3*). Using electrophysiology and behavior experiments in cannulated mice, we demonstrate that the EP3 agonist sulprostone acts more strongly in female mice to suppress tonic firing of LC neurons *ex vivo* and to specifically inhibit an LC-mediated stress response in females *in vivo*. Thus, we demonstrate previously unidentified sex differences in gene expression in NE neurons at a magnitude capable of influencing neurophysiology and pharmacologic responses. These molecular sex differences at the level of LC neurons may guide future investigations into models, mechanisms, or treatments for sex-skewed psychiatric diseases.

RESULTS

Generation and Validation of Reagents for Transcriptional Profiling of Noradrenergic Neurons

We generated a mouse line for transcriptional profiling of noradrenergic neurons by expressing EGFP/RPL10A from a NE reuptake transporter (*Slc6a2*) bacterial artificial chromosome (BAC). Neuroanatomical characterization revealed robust transgene expression in the A4 and A6 subdivisions of the LC (Figures 1A–1C), where EGFP/RPL10A perfectly co-localized with the LC-specific NE-synthesizing protein, DβH (Figure 1D), along with reasonably robust co-labeling in the A5 and A7 groups. EGFP/RPL10A labeling was weak and sparse in more caudal DβH+ populations (e.g., A1 and A2), consistent with prior immunofluorescence studies of SLC6A2 expression (Schroeter et al., 2000). Little EGFP expression was seen in ependymal cells, except rarely in cells caudal to the fourth ventricle (data not shown), in contrast to previously reported ependymal expression of SLC6A2. In total, this anatomical characterization asserts that mRNA collected by TRAP will be from the most robustly labeled and populous cells: the A4–A7 groups, predominantly the LC.

We then performed TRAP on two *Slc6a2* founder lines to evaluate consistency, to confirm enrichment of known LC-specific transcripts by TRAP, and to identify transcripts enriched in LC compared to the hindbrain. Reproducibility was strong between the lines (Pearson correlation > 0.99; Figure 1E). Relative to whole-hindbrain RNA from the same mice, TRAP enriched for genes with known specificity and functionality in the LC (Figure 1F), including (1) enzymes related to NE turnover (*Th*, *Ddc*, *Maoa*, and *Dbh*), (2) vesicular monoamine (*Slc18a2*) and NE (*Slc6a2*) transporters, (3) galanin (*Gal*) and its receptor (*GalR1*), and (4) a transcriptional regulator of LC development (*Phox2a*). After conservative filtering for expression and background, at least 3,139 transcripts were detected with high confidence in NE neurons; 526 were enriched >2-fold compared to hindbrain.

Gene Ontology (GO) analysis was applied to broadly characterize NE neuron-enriched transcripts, revealing enrichment of transmembrane receptors and ligands (Figure 1H), consistent with prior observations that CNS cell-type-specific genes often include receptors (Doyle et al., 2008). These LC-enriched receptors are highlighted (Table S1B), given the importance of the LC—and extrinsic modulation thereof—in behavior. Next, transcriptional profiles of LC and other CNS cell subtypes previously characterized by TRAP were compared to predict genes specific to the LC compared to other cells in the brain and the "transcriptional ontology" of the LC using our previously described pSI (specificity index p value) algorithm (see Experimental Procedures). Compared to all other available cell types, 162 genes scored as LC enriched (pSI < 0.05), with 78 highly so (pSI < 0.005) (Figure 2A; Table S1A). Hierarchical clustering placed noradrenergic cells with other neuromodulatory populations (Figure 1G), including serotonergic, hypocretinergic (Hcrt), and forebrain cholinergic neurons. The shared transcriptional relationship with Hcrt neurons is striking; despite their anatomic separation and the use of distinct neurotransmitters, they form reciprocal connections and share functional roles in control of sleep and arousal (reviewed in Carter et al., 2013), supporting the notion that gene expression in neuronal cell subtypes is a strong predictor of a subtype's functional roles.

Transcripts identified as LC enriched (Figure 2A) were then validated using standard RNA and protein detection methods in wild-type mice. *In situ* hybridization (ISH) for *Calcr* selectively and robustly stained the LC (Figure 2B), consistent with microarray results, suggesting very high enrichment of *Calcr* in the LC compared to hindbrain (over 300-fold). As the characteristic "quarter-moon" anatomy of the LC could be readily discerned by ISH, additional transcripts were systematically evaluated for enrichment using The Allen Brain Atlas (Figures 2C and S1). 70% of TRAP transcripts showed enriched *in situ* staining in the LC; over 19% scored as having "marker-like" expression. Finally, we confirmed protein translation in the the LC of several identified genes using immunofluorescence (Figure 2D).

Transcriptional Responses of NE Neurons to LPS Can Be Identified with *Slc6a2* TRAP

Having verified that TRAP characterizes baseline transcriptional features of the LC, we next sought to demonstrate the utility of this mouse line for profiling changes consequent to stimulation of the LC. LPS is a well-characterized example of an LC-activating stimulus: it strongly increases FOS expression in the LC,

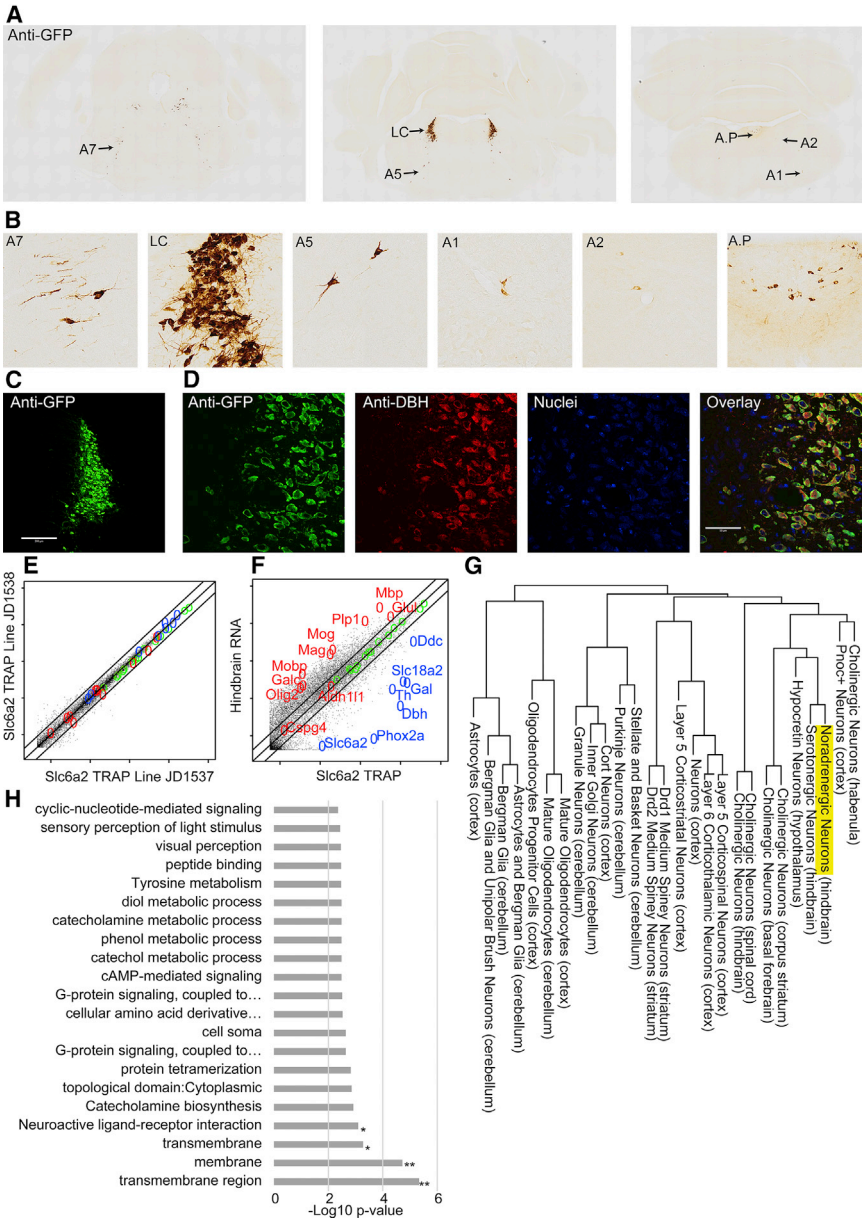

Figure 1. Characterization of Noradrenergic bacTRAP Lines

(A) Anti-GFP immunohistochemistry demonstrates EGFP/Rpl10a labeling in the hindbrain.

(B) Anti-GFP staining is most robust in anterior groups (A4–A7), especially LC.

(C) Immunofluorescence for GFP (green) labels entire LC. Scale bar, 200 μM.

(D) GFP co-labels completely with dopamine-β-hydroxylase (DBH) (red). Scale bar, 50 μM.

(E) Comparison of two *Slc6a2* TRAP lines demonstrates reproducibility.

(F) *Slc6a2* TRAP mRNA versus total hindbrain mRNA enriches NE neuron markers (blue) and depletes unrelated cell-type (glial) markers (red).

(E and F) Lines indicate 0.5-, 1-, and 2-fold. Log_{10} scale.

(G) Hierarchical clustering of *Slc6a2* neurons.

(H) *Slc6a2* TRAP enriches for transmembrane proteins and receptors. Hypergeometric test, Benjamini-Hochberg corrected; *p < 0.06; **p < 0.01.

See also Table S1B.

and the LPS-induced febrile response is lost with LC ablation (Almeida et al., 2004). Therefore, we injected individual TRAP mice with LPS or vehicle in a sex-balanced design. Whole-hindbrain RNA from the same lysates served as controls, as did a parallel TRAP experiment with *Slc6a4* TRAP mice targeting hindbrain serotonergic neurons (Figure 3).

We first examined whole-hindbrain changes in response to LPS (Figure 3B); 56 genes showed a response, predominantly upregulation (Table S1C). GO analysis identified a significant increase of interferon-induced transmembrane proteins (Figure S2), consistent with a broad pro-inflammatory transcriptional response. However, examination of *Slc6a2* TRAP revealed an even greater response (Figure 3C; Tables S1D and S1E), largely distinct from that of the hindbrain (only two genes were shared between hindbrain and LC). In contrast, response of serotonin neurons was limited (Figure 3B). Given the multitude of psychopharmacotherapeutics and environmental stimuli—including inflammation, pain, and acute stress—known to modulate the LC, these findings establish a useful system for identifying LC-specific molecular responses to whole-animal manipulations.

Noradrenergic Transcriptional Profiles Reveal Robust Sex Differences

To our surprise, sex-stratified analyses of these same experimental data revealed substantial sex differences in noradrenergic neurons. First, analysis of transcriptional profiles of the whole hindbrain varied remarkably little between sexes, with the exception of a few sex chromosomal genes (Figure 3C). Likewise, serotonin neurons showed no appreciable differences outside of sex chromosomal transcripts (e.g., *Ddx3y* and *Eif2s3y*). In contrast, noradrenergic neurons showed substantial molecular sex differences: a total of 152 transcripts were DEGs, most of which are autosomal (Figures 3D and 3E; Tables S1F and S1G), and these did not overlap with the serotonin neuron differential transcripts. These transcripts also do not significantly overlap with those stimulated by LPS, nor are they characterized by similar functional categories (Figure S2). This indicates that the observed molecular divergence is not likely due to sex differences in baseline activity level of the LC but rather reflects a more complex molecular distinction between the sexes. Motivated by the clear role of sex as a risk factor for psychiatric disorders, we focused on these sex differences for additional study.

A

Symbol	adj.P.Val	TRAP/Hind	pSI
Agtr1a	2.03E-04	46.3	6.15E-04
Asb4	3.95E-03	18.6	6.37E-06
Calcr	4.96E-04	457.9	6.37E-06
Calr3	9.99E-03	4.0	7.58E-04
Chodl	5.00E-04	20.8	7.01E-05
Chrna6	3.14E-04	45.7	6.37E-06
Cilp	4.83E-03	19.5	6.31E-04
Cyb561	5.83E-04	8.4	4.46E-05
Dbh	2.36E-04	161.8	6.37E-06
Ddc	2.84E-03	6.5	2.55E-05
Dlk1	3.22E-03	11.1	3.82E-05
Emr1	4.70E-04	139.8	6.37E-06
Eya2	3.14E-04	42.7	6.37E-06
Fam159b	2.54E-05	265.0	6.37E-06
Fam183b	4.83E-03	19.5	2.36E-04
Fibcd1	5.28E-03	22.3	2.87E-04
Gal	4.41E-04	57.4	6.37E-06
Gch1	9.63E-04	24.1	6.37E-06
Glra2	3.42E-03	7.0	2.04E-04
Gng4	2.54E-05	5.6	6.44E-04
Gpx3	1.68E-04	19.8	6.37E-06
Gtf2a1l	2.44E-03	49.5	2.55E-05
Hcrtr1	7.96E-04	27.0	6.37E-06
Igsf5	1.95E-03	82.6	6.37E-06
Maoa	3.79E-05	17.4	2.55E-05
Mrap2	5.54E-03	4.2	6.37E-06
Myom2	3.14E-04	198.3	6.37E-06
Neurog2	1.86E-02	21.6	2.74E-04
Nhedc2	3.25E-02	26.1	3.28E-04
Nxph4	6.68E-03	17.4	4.01E-04
Ovgp1	1.33E-02	33.7	6.37E-06
Pcbd1	3.14E-04	10.4	3.19E-05
Phox2a	3.37E-05	265.9	6.37E-06
Phox2b	9.51E-03	2.2	7.58E-04
Pla2g4d	6.12E-05	21.1	4.33E-04
Ptger2	8.53E-04	13.6	2.48E-04
Slc18a2	2.37E-03	42.5	6.37E-06
Slc31a1	3.15E-03	5.6	5.10E-04
Slc6a2	1.81E-04	21.7	1.72E-04
Stbd1	1.03E-03	41.3	5.48E-04
Syt17	4.18E-03	134.9	1.27E-05
Th	2.44E-03	36.6	6.37E-06
Tm4sf1	2.14E-03	6.0	7.01E-05
Tm4sf5	1.47E-03	27.1	1.43E-04
Traf3ip2	1.23E-03	14.5	6.37E-05

B

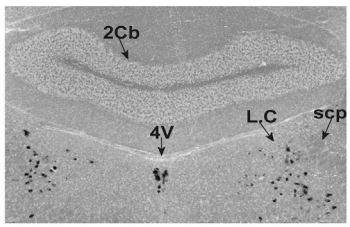

C

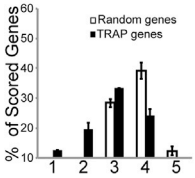

#	Description	Examp.
1	Specific w/in brain	Dbh
2	Specific w/in region	Th
3	Enriched in LC	Phox2b
4	Broadly exp., inc. LC	Actb
5	Clearly not in LC	Pcp2

D

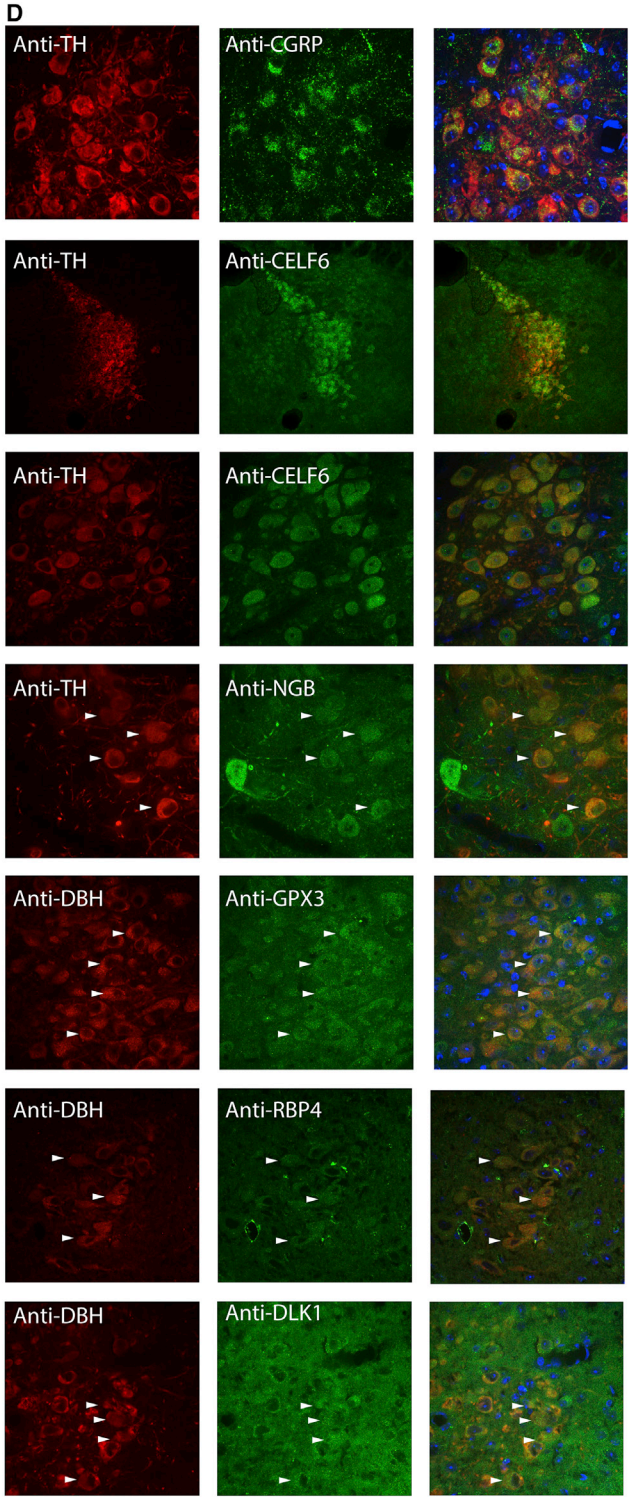

Figure 2. Transcript and Protein Expression in LC Neurons

(A) Top 45 named genes enriched by TRAP over hindbrain (adjusted p value), fold change (TRAP/Hind), and specificity index p value (pSI) comparing *Slc6a2* to all cell populations from Figure 1G (see also Table S1A).

(B) ISH confirms LC enrichment of calcitonin receptor. 4V, fourth ventricle; scp, superior cerebellar peduncle; 2cb, cerebellar vermis.

(legend continued on next page)

Sex-Differential LC Genes and Putative *cis*-Regulators Implicated in Disease and Behavior

As a preliminary investigation into possible gene-regulatory mechanisms underlying sex differences in LC gene expression, we characterized DNA sequence motifs in *cis* with these 152 genes. Performing *de novo* motif discovery for DEGs from each sex, we identified 12 motifs (Table S2). Compared to their frequency near 1,000 randomly selected genes, six of these were significantly enriched near the DEGs. Thus, at least a portion of the sex differences in gene expression could be explained by conserved *cis*-regulatory elements in the surrounding genome. Known transcription factor binding sites predicted in these motifs included *OTX2*, *NR2F6*, and *MTF1* (Table S2).

Molecular Differences Predict Functional Differences between Sexes

Finally, we noted LC specificity and female LC enrichment (>2-fold; Table S1E) of the *Ptger3* gene, encoding the prostaglandin E2 (PGE2) receptor EP3. Given the specificity of this gene's expression to the LC (Table S1A) within the hindbrain and the existence of a known, selective agonist, sulprostone, we selected EP3 to pharmacologically test whether the magnitudes of detected sex differences in receptor gene expression were adequate to alter LC electrophysiology and/or behavior.

We first assessed whether pharmacologic manipulation of the EP3 receptor resulted in sex-differential electrophysiologic responses by performing whole-cell recordings from LC neurons in *ex vivo* slices. EP3 presence in the LC was confirmed—and subsequently manipulated—by bath application of sulprostone (agonist), followed by L798,106 (antagonist) to displace sulprostone, halting its effects. Sulprostone suppressed baseline tonic firing of LC neurons in both sexes, but with a greater magnitude and duration of hyperpolarization in female LC compared to male LC (Figures 4A and 4B). Voltage-clamp recordings from a second cohort of mice revealed a larger outward current from female LC neurons (Figures 4C and 4D), verifying that the magnitude of LC inhibition by EP3 corresponds to sex differences in *Ptger3* expression.

We previously showed in male mice that LC silencing with Gi-coupled designer receptors exclusively activated by designer drugs (DREADDs) prevents anxiety-like behavior in the open-field task (OFT) after restraint stress (McCall et al., 2015). This behavioral paradigm provided a robust model system in which we could activate the LC *in vivo*, and subsequently attempt to suppress the LC pharmacologically, with behavior as the outcome measure. We first validated that restraint stress robustly induces anxiety-like behavior (avoidance of center) in the OFT in mice of both sexes (Figures 4E and 4H). Restraint stress did not impact total activity or the sex difference therein but clearly induced avoidance of center in both sexes. Thus, we hypothesized that EP3 agonists could be used to reduce stress-induced anxiety, specifically in wild-type female mice. Indeed, administration of sulprostone via cannula to male and female LC immediately before restraint stress and OFT resulted in selectively reduced anxiety-like behavior in females (Figures 4I–4L). Post hoc analysis of phosphorylated-FOS (p-FOS) expression in TH+ neurons of the LC in the same animals revealed similar staining intensity of p-FOS and numbers of double-positive cells between sexes (data not shown). The robust immediate-early response in both conditions is consistent with intact stimulation of LC neurons by stress, suggesting that sulprostone inhibits noradrenergic output. Sulprostone did not affect the baseline sex difference in total ambulatory activity. (Figure 4M).

DISCUSSION

Characterizing gene expression in noradrenergic neurons—regardless of whether they are at the etiologic root of neuropsychiatric diseases and disease models—is key to narrowing down possible mechanisms by which NE signaling may be dysregulated in disease states. We have presented a mouse line enabling transcriptional profiling of LC neurons at baseline and after physiologic manipulations (LPS). In characterizing this line, we discover and herein report a breadth of previously unidentified sex differences in molecular features of the mouse LC. These findings highlight the LC as an area of focus for future studies in neuropsychiatry, especially in domains where sex differences are observed in modeled behaviors or diseases. In contrast, we find that serotonergic neurons show few sex differences in gene expression, despite their hypothesized role in behavior and psychiatric disease. Sex-differential expression of one such receptor, PTGER3, was adequate in magnitude to sex-differentially affect electrophysiologic and behavioral pharmacologic responses. This independent verification of our transcriptomic findings suggests that sex-differentially expressed genes in the LC (1) may underlie sex differences in behavior and behavioral pathology and (2) can be targeted to sex-specifically modulate LC-mediated behaviors. Thus, we conclude that the LC is an interesting candidate for mediating sex differences in monoamine-associated psychiatric phenotypes. We further envision that this mouse line could provide an invaluable tool in studies aimed at identifying mechanisms of existing NE-targeting drugs at the transcriptomic level and enable prioritization of new, precise drug targets aimed at the same transcriptional endpoints.

Our profiling extends previous work illustrating discrete molecular sex differences in the LC. Perhaps best characterized is the trafficking of receptor CRF1 and response to its ligand, CRF (Bangasser et al., 2016; Curtis et al., 2006; Valentino et al., 2012). Likewise, the expression of the μ-opioid receptor and response to opioid agonism in the LC shows a sex difference (Guajardo et al., 2016). Estrogen regulates genes required for NE synthesis in a sex-specific fashion (discussed later). Structural dimorphism in the rat LC has also been observed, though the direction of effect depends on the strain of rat (compare Babstock et al., 1997; Bangasser et al., 2011; and Luque et al., 1992). Finally, postnatal citalopram exposure in rats causes ectopic

(C) Blind comparison of TRAP-identified and random genes confirms TRAP transcript presence in LC ($p < 2.7E-38$, chi-square test, normalized to number of n = 53 TRAP-identified transcripts and 94 randomly selected transcripts). Error bars are ± SEM for two independent, blinded scorers (see also Figure S1).
(D) Immunofluoresence confirms translation of TRAP-identified transcripts (green) in LC cells (arrowheads), labeled by either TH or DBH (red).
See also Figure S1 and Table S1A.

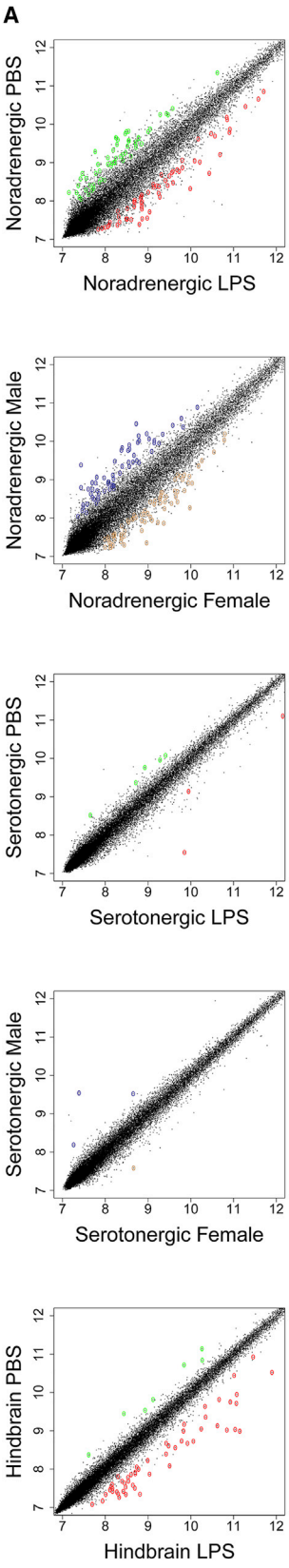

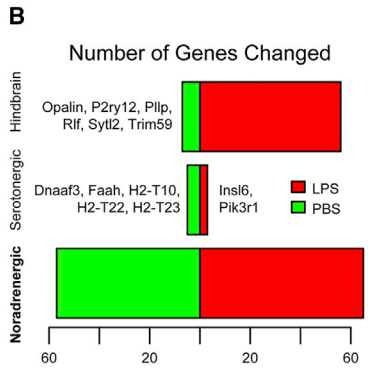

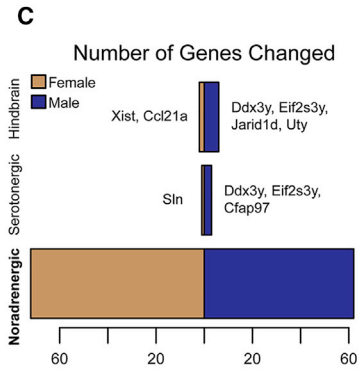

D

Gene Symbol	p.value	F/M	TRAP / Hind
Arfgap1	0.025	1.93	1.33
Arg2	0.034	1.58	1.33
Atp6v1a	0.029	1.93	1.61
Cd151	0.008	2.63	3.01
Cd200	0.030	2.33	1.56
Dgkb	0.006	1.64	1.59
Dguok	0.025	1.97	1.32
Disp1	0.042	2.12	1.07
Dnaja3	0.005	1.55	1.53
Dzip1l	0.046	1.82	1.05
Eif2s2	0.002	1.75	1.04
Elavl4	0.000	2.05	1.53
Fpgs	0.039	1.61	1.34
Gabre	0.027	1.51	2.12
Gga2	0.012	2.01	1.18
Gipc1	0.017	2.54	3.23
Golt1b	0.009	1.60	1.88
Gosr2	0.043	1.76	2.17
H13	0.003	1.52	2.13
Hbs1l	0.040	1.74	1.65
Lin28b	0.027	1.53	1.52
Mrps11	0.007	1.66	2.34
Nat14	0.022	2.13	2.59
Nfu1	0.042	1.56	1.23
Nkrf	0.023	1.74	1.06
Nt5dc2	0.026	1.89	2.21
Pacrg	0.046	2.12	1.35
Peg10	0.019	1.68	3.64
Pja1	0.043	1.86	1.46
Polm	0.037	1.75	1.60
Ptger3	0.001	2.28	3.07
Ptrh2	0.037	1.63	1.18
Raph1	0.016	1.70	1.43
Sec22a	0.031	1.73	1.52
Sf3b2	0.002	1.78	1.16
Sgip1	0.030	1.78	1.38
Slc6a15	0.028	1.60	0.88
Snhg12	0.015	3.04	2.26
Srd5a3	0.029	1.98	1.87
Stx17	0.009	1.60	1.41
Tbc1d19	0.039	1.62	1.03
Tcea3	0.006	1.76	1.48
Tcf12	0.024	3.67	1.20
Tead1	0.000	2.22	0.92
Tex9	0.000	2.23	0.99
Tiam1	0.035	2.15	0.92
Tm7sf3	0.029	3.40	1.73
Ubxn7	0.046	1.94	1.09
Vrk1	0.037	1.59	1.30

E

Gene Symbol	p.value	M / F	TRAP / Hind
Alg10b	0.003	2.37	2.26
Ap2a2	0.013	1.63	1.59
Arhgef6	0.031	1.93	1.04
Armc8	0.028	1.77	1.21
Atp6ap2	0.028	1.51	1.46
Atrx	0.025	2.34	0.97
Ccl17	0.029	1.66	2.43
Cep250	0.019	1.85	0.87
Chkb	0.023	1.59	0.99
Dapk2	0.033	2.80	0.92
Dedd	0.004	1.58	1.58
Dok4	0.005	2.44	1.68
Dpysl2	0.034	1.49	1.15
Dstyk	0.038	1.49	0.88
Elp3	0.035	1.90	1.14
Epn2	0.040	1.96	0.90
Ftl1	0.036	1.77	1.85
Gnas	0.031	1.59	1.29
Hk2	0.037	2.84	2.32
Hrasls	0.045	1.87	1.38
Igf1r	0.021	1.81	1.10
Inppl1	0.003	2.37	1.26
Kmt5c	0.045	1.86	1.83
Ldlr	0.045	2.69	3.06
Metrn	0.023	3.70	0.99
Mtf1	0.022	2.83	1.25
Nfat5	0.006	2.10	0.95
Ntrk3	0.024	2.20	1.18
Patz1	0.004	2.37	1.61
Pex14	0.011	1.67	1.61
Ppcdc	0.031	1.61	1.61
Rab5a	0.020	2.13	1.19
Rrp9	0.036	2.02	1.92
Rtn1	0.042	1.71	1.49
Slc36a1	0.019	1.79	2.05
Slc7a7	0.043	1.80	1.84
Slc9a3r2	0.040	1.84	0.88
Slc9a6	0.005	1.62	1.35
Smim11	0.021	1.97	1.59
Spata13	0.017	2.28	1.42
Srprb	0.039	2.54	2.43
Tada3	0.047	1.71	1.20
Tanc2	0.034	1.81	1.31
Tipin	0.015	1.81	1.05
Tmtc2	0.003	1.57	1.41
Tubgcp4	0.046	2.55	1.42
Ube2o	0.031	1.82	1.03
Uqcc1	0.006	1.81	1.75
Xrn2	0.025	1.88	0.86

(legend on next page)

projection of LC fibers into the neocortex and increased LC excitability in males, but not females (Darling et al., 2011). We expand upon this body of research by identifying thousands of genes expressed in the LC and sex differences therein, as well as recurrent, conserved motifs in *cis* with these genes.

Among the transcripts with sex differences identified in the LC, we identified a number of genes and putative *cis*-regulators notable for their previous implications in behavior and brain development. Putative regulators in *cis* with the DEGs included three striking candidates: OTX2, NR2F6, and MTF1. OTX2 was recently shown to regulate depression-related consequences of early life stress in male mice (females were untested) through actions in dopaminergic neurons (Peña et al., 2017). MTF1 is notable for its role in binding and responding to heavy metals, perturbations of which have been implicated in ASDs (Arora et al., 2017; Hagmeyer et al., 2015); furthermore, this transcription factor was itself enriched in the LC of males, providing hints of a potential regulator of some of our observed sex differences. Finally, NR2F6 is a nuclear receptor known to be required for LC differentiation, consistent with LC enrichment of the genes used for motif analysis. As the motif analysis only utilized conserved regions of mammalian sequence near these genes, these regulatory mechanisms—and, thus, sex differences—may be conserved in humans.

Intriguingly, we also noted a previously unidentified female enrichment PGE2 receptor *Ptger3* (EP3) in the LC. PGE2 and PTGER family receptors are known to mediate sexually dimorphic neurodevelopment in the preoptic area of the hypothalamus (Amateau and McCarthy, 2004; Wright et al., 2008); sex-differential expression of these receptors in a separate, adult brain region was, thus, intriguing. The enrichment of PGE2 receptors is interesting in the context of LPS, which we used here to stimulate the LC, but also stimulates fever; PGE2 and the LC are major effectors of LPS-induced fever via the EP3 and EP4 receptors (Almeida et al., 2004; Oka et al., 2000). Follow-up studies are merited to explore whether the EP3 receptor plays a role in fever effects on behavior via the LC and whether its differential expression is the cause or consequence of the broader transcriptomic sex differences presented here.

This expression difference was sufficient to modulate behavior in a sex-specific way, which we validated by LC-targeted pharmacologic manipulation. Using sulprostone to agonize EP3, we identified strong inhibitory effects on LC firing in female LC neurons, consistent with the pattern of its increased female expression. We then utilized restraint stress as a validated means of activating the LC and triggering LC-mediated behavioral changes (McCall et al., 2015, 2017; Seo and Bruchas, 2017; Uematsu et al., 2017). In turn, we aimed to suppress restraint-driven LC activation by administering sulprostone beforehand, ameliorating behavioral signs of stress-induced LC activity in female, but not male, mice. Thus, we demonstrate that the sex differences in receptor expression measured in the LC by TRAP are of an adequate magnitude to manipulate an LC-regulated behavior in a sex-specific manner.

Our stress paradigm was only used to robustly activate the LC, rather than to investigate stress per se. Whether EP3 plays a role in—or undergoes transcriptional or translational regulation in response to—physiologic sex differences in the stress response of the LC remains unclarified. We also note that the mice in which DEGs were identified were singly housed (potentially a stressor, i.e., social isolation), and housed at an unstressful, thermonormal 30°C for fever experiments. We note, however, that our electrophysiologic and behavioral findings regarding PTGER3 were consistent with the observed expression changes, despite the mice for the later experiments being group-housed at a normal room temperature. Using these TRAP mice to deliberately study sex-specific transcriptional/translational responses to stress will be an interesting application of this mouse line in future investigations.

It is interesting to speculate that sex differences in LC gene expression may specifically influence increased female risk of disorders like GAD and MDD, where NE-modulating drugs have seen use for decades. If higher baseline expression of some genes in the female LC promotes risk for MDD, then common variants that elevate the expression of those same genes may likewise confer depression risk. Indeed, when we examined the 15 documented MDD-associated loci (Hyde et al., 2016) for the presence of sex-differential LC genes, we found two genes associated with MDD are enriched in LC of female mice: *Slc6a15* and *Lin28b.* This striking coincidence may imply that certain sex- and variant-mediated MDD risk factors converge in the LC. Future research is warranted to explore whether sex- and disease-associated regulatory variants concordantly affect gene expression and psychiatric disease risk via LC and other monoamingergic cell populations.

Overall, the marked molecular sex differences present interesting areas for future inquiry. Most notably, the mechanism of establishing these sex differences (hormonal-developmental, sex-chromosomal, or post-pubertal hormonal) remains unclarified. Previous work has shown that estrogen regulates the expression of *Th* and *Dbh*—and, thus, NE synthesis—in a sex-differential manner in adult rodents (Serova et al., 2002; Thanky et al., 2002). In the present study, estrous cycling was not examined for effects on transcriptional sex differences. Regarding behavior, we note that estrous cycling does not appear to play a role in most behaviors (Prendergast et al., 2014), including center time in the open field task for C57BL6 mice (Meziane et al., 2007); binning behavior data by estrus stage revealed no substantial differences (Figure S4). Another possible mechanism, the perinatal masculinizing hormonal surge in male rodents that organizes other dimorphic regions, might be equally

Figure 3. Differentially Expressed Genes by Sex

(A–C) Scatterplots contrasting transcriptional data between LPS and vehicle (PBS) or sex (A); DEGs are indicated by color. (B and C) Number of DEGs after LPS (B) (red, up; green, down) or between vehicle-treated sexes (C) in each sample type (see also Tables S1C–S1G).

(D and E) Top 50 named sex-DEGs in LC of females (D) or males (E). M/F or F/M represents fold change between sexes; TRAP/Hind represents fold change, TRAP versus hindbrain.

See also Figure S2 and Tables S1C–S1G.

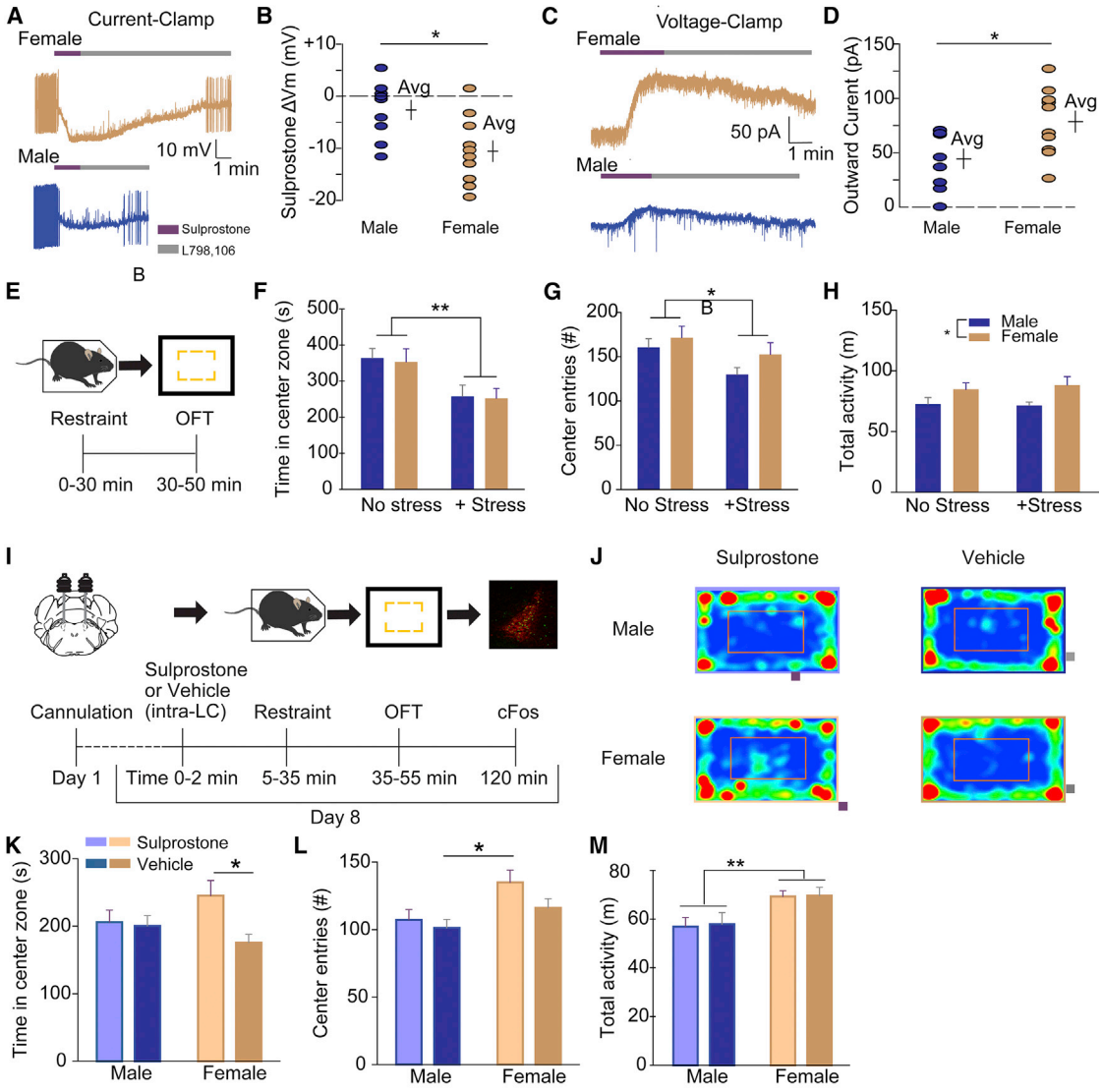

Figure 4. Sex Differences in *Ptger3* Expression Can Be Reflected in LC-Mediated Behavior

(A–C) Representative current-clamp (A) and voltage-clamp (C) traces from LC slices exposed to sulprostone (200 nM), followed by L798,106 (300 nM).

(B) Maximum change in membrane voltage (mV) after sulprostone, by sex (−10.5 ± 2.1 mV, n = 10 cells from 5 females; −2.6 ± 1.8 mV, n = 9 cells from 4 males; $p < 0.05$, Mann-Whitney).

(D) Maximum change in outward current (pA) after sulprostone, by sex (78.5 ± 9.7 pA, n = 10 cells from 3 females; 44.4 ± 8.9 pA, n = 9 cells from 3 males; $p < 0.05$, Mann-Whitney).

(E) Schematic of validated stress-anxiety paradigm.

(F–H) Effects of restraint stress on OFT task performance (n = 6–7).

(F) Time in center zone.

(G) Center entries.

(H) Total activity.

(I) Timeline of LC pharmacology-behavior experiments.

(J) Representative OFT traces from each sex and treatment condition.

(K and L) Sulprostone administration prevents stress-induced anxiety in female (ns = 17 and 17) but not male (ns = 16 and 14) mice in OFT; time (K) and center zone entries (L) (see also Figure S4 for estrous-stage-specific behaviors).

(M) Time in center was unaffected by sulprostone for both sexes.

*$p < 0.05$; **$p < 0.01$. All error bars indicate SEM.

See also Figure S4.

important in the LC—indeed, structural differences in female rat LC can be attenuated by perinatal testosterone administration (Guillamón et al., 1988). Overall, it is possible that multiple mechanisms contribute to the molecular sex differences we detected. Thus, future studies are warranted, both focusing on identifying these mechanisms and examining the potential conservation of these differences.

EXPERIMENTAL PROCEDURES

Animal Research Statement

All procedures involving animals were approved by the institutional animal care and use committees of Rockefeller University, Case Western Reserve University, and Washington University in St. Louis, MO.

Immunofluorescence Microscopy

Paraformaldehyde (PFA)-perfused mouse brains were dissected, cryoprotected, and cut by cryostat into floating sections for immunostaining with primary antibodies and Alexa fluorophore-labeled secondary antibodies. Antibodies used are described in Table S1J.

TRAP for Initial Description of LC

Replicate pools of five mixed-sex adult mice from each of the *Slc6a2* lines were sacrificed. Brains were removed for collection of hindbrain posterior to the pontine/hypothalamic junction (discarding the cerebellum).

All array data were analyzed in R using Bioconductor packages. *GCRMA* was used to normalize within replicates and to biotinylated spike-in probes (green dots, Figure 1F) between conditions. Fold change, specificity index (SI), and pSI were calculated for genes expressed above non-specific background, defined as at least 2 SDs above the mean TRAP:hindbrain ratio of negative control transcripts (Figure 1F, red dots). LC-enriched transcripts were identified using the empirical Bayesian statistic with false discovery rate (FDR) correction in *limma*. The pSI algorithm was used with default settings to compare LC TRAP cells to other cells profiled by TRAP (Figure 1G). Hierarchical clustering across cell types was conducted in R, utilizing expression values from genes with pSI < 0.01 in any cell type.

Scoring of The Allen Brain Atlas for LC Gene Specificity

Any transcript that scored between 1 and 3 (examples in Figure S1**)** was considered to be marker-like. A chi-square test was performed, comparing the observed counts of each score with expected counts (based on the random gene set) for each score.

Single-Animal TRAP for Sex-Differential and LPS-Responsive Gene Expression

Samples were prepared and hybridized in two batches counterbalanced for mouse strain, sex, and LPS. After processing, one *Slc6a4* TRAP sample and two hindbrain samples were excluded due to poor hybridization. Remaining samples were normalized using the *lumi* package. Appropriate clustering of replicates was confirmed with multidimensional scaling (MDS) plots (Figure S5). Differential expression was defined as $p < 0.05$ on a paired t test (paired on batch and covariate), and $\log_2$ fold change of $\pm$ 0.585 across 3 of 4 paired comparisons. For balance, the single *Slc6a4* replicate was used twice to replace the low-quality sample. (Results are given in Tables S1C–S1G.)

To validate this analytic approach, we performed standard differential expression analysis in *limma*. Resulting p values for genes identified in the former analysis in Tables S1C–S1G. Full array results from this analysis are given in Table S3. The two analyses and locations of their results are also given in Table S1K.

Motif Analysis of Peri-TSS Sequences of Sex-DEGs in LC

For each sex-differentially expressed gene identified in the LC (Tables S1F and S1G), mm10 genomic sequences 10 kb 5′ and 10 kb 3′ to the transcription start site (TSS) were acquired. Exonic bases in non-conserved regions of sequence (based on PhyloP scores) were masked out. Masked flanking sequences were submitted to MEME (Bailey et al., 2015) for *de novo* discovery of motifs 8–20 bp long. The associated tool, TomTom, was used to compare motifs to known transcription factor (TF) binding sites (Kulakovskiy et al., 2018; Mathelier et al., 2016; Weirauch et al., 2014). Motif frequency, consensus sequence, and predicted TFs discussed in the text are provided (Table S2). To assess motif enrichment near LC transcripts, 1,000 random protein-coding TSSs were selected and processed identically. These were searched for motif matches using FIMO at the same p cutoff for a "match" used by MEME during discovery. The number of unique loci containing $\geq$1-motif match among all loci was then compared using chi-square analysis, followed by Benjamini-Hochberg correction.

Electrophysiology of LC Neurons Exposed to PTGER3 Agonist/Antagonist

Whole-cell recordings were made using an Axopatch 200B amplifier (Molecular Devices). LC neurons were identified by location, capacitance > 40 pF, an input resistance < 100 MΩ, and a tonic firing rate of 0.5–4 Hz.

Stereotaxic Cannulation of LC

Mice were allowed to recover from surgery 7–9 days prior to behavioral testing. Animals were also habituated to handling and connection to tubing for 3 consecutive days prior to behavioral testing.

Stress-Induced Anxiety Behavioral Paradigm

Anymaze was used for video recording of animal movements for center and periphery analysis. The center zone was defined as a concentric rectangle comprising 50% of the OFT area. Cannula placement was confirmed by cryostat sectioning of perfused brains (Figure S3) to determine mice for inclusion in the final behavioral and p-FOS analyses.

c-FOS Quantification in LC following Sulprostone/Vehicle, Restraint, and OFT

Gain, light intensity, and exposure time were identical for all prepared microscope slides. Using ImageJ, background was subtracted, ROIs were made around the LC based on tyrosine hydroxylase (TH) staining, and average pixel intensity for p-FOS fluorescence was measured. p-FOS-TH double-positive cells were counted manually by a blinded experimenter.

DATA AND SOFTWARE AVAILABILITY

The accession number for the transcriptomic data reported in this paper is GEO: GSE100005 (https://www.ncbi.nlm.nih.gov/geo/).

SUPPLEMENTAL INFORMATION

Supplemental Information includes Supplemental Experimental Procedures, five figures, and three tables and can be found with this article online at https://doi.org/10.1016/j.celrep.2018.04.054.

ACKNOWLEDGMENTS

The authors thank R. Jaswany, E. Park, C. Jakes, K. McCullough, and L. Broestl for assistance in performing lab experiments; K. Nygaard for editorial assistance; T.C. Mazer for discussion of potential hormonal mechanisms of these findings; and the Rockefeller University Genomics Resource Center and Bioimaging Cores. This work was supported by the NIH (5R01HG008687, 4R00NS067239, 5R21DA038458, R01DA035821, and R01NS095809), the Simons Foundation, the Brain and Behavior Research Foundation, Ludwig Cancer Research, BBSRC (BB/M001873/1), and a CDI Microgrant from the Washington University Center for Cellular Imaging (WUCCI).

AUTHOR CONTRIBUTIONS

Conceptualization: J.D.D., N.H., and B.M; Methodology: J.D.D., S.K., N.H.; Validation: J.D.D., B.M., and D.L.B.; Formal Analysis: J.D.D., A.M.L., and

B.M.; Investigation: J.D.D., B.M., D.L.B., S.K., S.G., and C.P.F.; Resources: J.D.D., M.R.B., C.P.F., and N.H.; Data Curation: J.D.D. and A.M.L.; Writing: B.M. and J.D.D.; Visualization: J.D.D., D.L.B., B.M., A.M.L., and C.P.F.; Supervision: N.H., J.D.D., and M.R.B.; Project Administration: J.D.D., B.M., and M.R.B.; Funding Acquisition: N.H., M.R.B., and J.D.D.

DECLARATION OF INTERESTS

J.D.D. has previously received royalties for patents related to TRAP technology. The remaining authors declare no competing interests.

Received: August 25, 2017
Revised: February 23, 2018
Accepted: April 13, 2018
Published: May 22, 2018

REFERENCES

Almeida, M.C., Steiner, A.A., Coimbra, N.C., and Branco, L.G.S. (2004). Thermoeffector neuronal pathways in fever: a study in rats showing a new role of the locus coeruleus. J. Physiol. *558*, 283–294.

Amateau, S.K., and McCarthy, M.M. (2004). Induction of PGE2 by estradiol mediates developmental masculinization of sex behavior. Nat. Neurosci. *7*, 643–650.

Arora, M., Reichenberg, A., Willfors, C., Austin, C., Gennings, C., Berggren, S., Lichtenstein, P., Anckarsäter, H., Tammimies, K., and Bölte, S. (2017). Fetal and postnatal metal dysregulation in autism. Nat. Commun. *8*, 15493.

Babstock, D., Malsbury, C.W., and Harley, C.W. (1997). The dorsal locus coeruleus is larger in male than in female Sprague-Dawley rats. Neurosci. Lett. *224*, 157–160.

Bailey, T.L., Johnson, J., Grant, C.E., and Noble, W.S. (2015). The MEME suite. Nucleic Acids Res. *43* (*W1*), W39–W49.

Bangasser, D.A., Zhang, X., Garachh, V., Hanhauser, E., and Valentino, R.J. (2011). Sexual dimorphism in locus coeruleus dendritic morphology: a structural basis for sex differences in emotional arousal. Physiol. Behav. *103*, 342–351.

Bangasser, D.A., Wiersielis, K.R., and Khantsis, S. (2016). Sex differences in the locus coeruleus-norepinephrine system and its regulation by stress. Brain Res. *1641* (*Pt B*), 177–188.

Carter, M.E., de Lecea, L., and Adamantidis, A. (2013). Functional wiring of hypocretin and LC-NE neurons: implications for arousal. Front. Behav. Neurosci. *7*, 43.

Christensen, D.L., Baio, J., Van Naarden Braun, K., Bilder, D., Charles, J., Constantino, J.N., Daniels, J., Durkin, M.S., Fitzgerald, R.T., Kurzius-Spencer, M., et al.; Centers for Disease Control and Prevention (CDC) (2016). Prevalence and characteristics of autism spectrum disorder among children aged 8 years–Autism and Developmental Disabilities Monitoring Network, 11 sites, United States, 2012. MMWR Surveill. Summ. *65*, 1–23.

Curtis, A.L., Bethea, T., and Valentino, R.J. (2006). Sexually dimorphic responses of the brain norepinephrine system to stress and corticotropin-releasing factor. Neuropsychopharmacology *31*, 544–554.

Darling, R.D., Alzghoul, L., Zhang, J., Khatri, N., Paul, I.A., Simpson, K.L., and Lin, R.C.S. (2011). Perinatal citalopram exposure selectively increases locus ceruleus circuit function in male rats. J. Neurosci. *31*, 16709–16715.

Doyle, J.P., Dougherty, J.D., Heiman, M., Schmidt, E.F., Stevens, T.R., Ma, G., Bupp, S., Shrestha, P., Shah, R.D., Doughty, M.L., et al. (2008). Application of a translational profiling approach for the comparative analysis of CNS cell types. Cell *135*, 749–762.

Fombonne, E. (2009). Epidemiology of pervasive developmental disorders. Pediatr. Res. *65*, 591–598.

Guajardo, H.M., Snyder, K., Ho, A., and Valentino, R.J. (2016). Sex differences in μ-opioid receptor regulation of the rat locus coeruleus and their cognitive consequences. Neuropsychopharmacology *42*, 1295–1304.

Guillamón, A., de Blas, M.R., and Segovia, S. (1988). Effects of sex steroids on the development of the locus coeruleus in the rat. Brain Res. *468*, 306–310.

Hagmeyer, S., Mangus, K., Boeckers, T.M., and Grabrucker, A.M. (2015). Effects of trace metal profiles characteristic for autism on synapses in cultured neurons. Neural Plast. *2015*, Article ID 985083.

Hare, A.S., Clarke, G., and Tolchard, S. (1995). Bacterial lipopolysaccharide-induced changes in FOS protein expression in the rat brain: correlation with thermoregulatory changes and plasma corticosterone. J. Neuroendocrinol. *7*, 791–799.

Hyde, C.L., Nagle, M.W., Tian, C., Chen, X., Paciga, S.A., Wendland, J.R., Tung, J.Y., Hinds, D.A., Perlis, R.H., and Winslow, A.R. (2016). Identification of 15 genetic loci associated with risk of major depression in individuals of European descent. Nat. Genet. *48*, 1031–1036.

Kessler, R.C., Berglund, P., Demler, O., Jin, R., Merikangas, K.R., and Walters, E.E. (2005). Lifetime prevalence and age-of-onset distributions of DSM-IV disorders in the National Comorbidity Survey Replication. Arch. Gen. Psychiatry *62*, 593–602.

Kulakovskiy, I.V., Vorontsov, I.E., Yevshin, I.S., Sharipov, R.N., Fedorova, A.D., Rumynskiy, E.I., Medvedeva, Y.A., Magana-Mora, A., Bajic, V.B., Papatsenko, D.A., et al. (2018). HOCOMOCO: towards a complete collection of transcription factor binding models for human and mouse via large-scale ChIP-Seq analysis. Nucleic Acids Res. *46* (*D1*), D252–D259.

Kurosawa, N., Shimizu, K., and Seki, K. (2016). The development of depression-like behavior is consolidated by IL-6-induced activation of locus coeruleus neurons and IL-1β-induced elevated leptin levels in mice. Psychopharmacology (Berl.) *233*, 1725–1737.

Luque, J.M., de Blas, M.R., Segovia, S., and Guillamón, A. (1992). Sexual dimorphism of the dopamine-β-hydroxylase-immunoreactive neurons in the rat locus ceruleus. Brain Res. Dev. Brain Res. *67*, 211–215.

Mathelier, A., Fornes, O., Arenillas, D.J., Chen, C.-Y., Denay, G., Lee, J., Shi, W., Shyr, C., Tan, G., Worsley-Hunt, R., et al. (2016). JASPAR 2016: a major expansion and update of the open-access database of transcription factor binding profiles. Nucleic Acids Res. *44* (*D1*), D110–D115.

McCall, J.G., Al-Hasani, R., Siuda, E.R., Hong, D.Y., Norris, A.J., Ford, C.P., and Bruchas, M.R. (2015). CRH engagement of the locus coeruleus noradrenergic system mediates stress-induced anxiety. Neuron *87*, 605–620.

McCall, J.G., Siuda, E.R., Bhatti, D.L., Lawson, L.A., McElligott, Z.A., Stuber, G.D., and Bruchas, M.R. (2017). Locus coeruleus to basolateral amygdala noradrenergic projections promote anxiety-like behavior. eLife *6*, 2837.

Meziane, H., Ouagazzal, A.-M., Aubert, L., Wietrzych, M., and Krezel, W. (2007). Estrous cycle effects on behavior of C57BL/6J and BALB/cByJ female mice: implications for phenotyping strategies. Genes Brain Behav. *6*, 192–200.

Oka, T., Oka, K., Scammell, T.E., Lee, C., Kelly, J.F., Nantel, F., Elmquist, J.K., and Saper, C.B. (2000). Relationship of EP(1-4) prostaglandin receptors with rat hypothalamic cell groups involved in lipopolysaccharide fever responses. J. Comp. Neurol. *428*, 20–32.

Peña, C.J., Kronman, H.G., Walker, D.M., Cates, H.M., Bagot, R.C., Purushothaman, I., Issler, O., Loh, Y.E., Leong, T., Kiraly, D.D., et al. (2017). Early life stress confers lifelong stress susceptibility in mice via ventral tegmental area OTX2. Science *356*, 1185–1188.

Prendergast, B.J., Onishi, K.G., and Zucker, I. (2014). Female mice liberated for inclusion in neuroscience and biomedical research. Neurosci. Biobehav. Rev. *40*, 1–5.

Sara, S.J. (2009). The locus coeruleus and noradrenergic modulation of cognition. Nat. Rev. Neurosci. *10*, 211–223.

Schroeter, S., Apparsundaram, S., Wiley, R.G., Miner, L.H., Sesack, S.R., and Blakely, R.D. (2000). Immunolocalization of the cocaine- and antidepressant-sensitive l-norepinephrine transporter. J. Comp. Neurol. *420*, 211–232.

Seo, D.O., and Bruchas, M.R. (2017). Polymorphic computation in locus coeruleus networks. Nat. Neurosci. *20*, 1517–1519.

Serova, L., Rivkin, M., Nakashima, A., and Sabban, E.L. (2002). Estradiol stimulates gene expression of norepinephrine biosynthetic enzymes in rat locus coeruleus. Neuroendocrinology *75*, 193–200.

Thanky, N.R., Son, J.H., and Herbison, A.E. (2002). Sex differences in the regulation of tyrosine hydroxylase gene transcription by estrogen in the locus coeruleus of TH9-LacZ transgenic mice. Brain Res. Mol. Brain Res. *104*, 220–226.

Uematsu, A., Tan, B.Z., Ycu, E.A., Cuevas, J.S., Koivumaa, J., Junyent, F., Kremer, E.J., Witten, I.B., Deisseroth, K., and Johansen, J.P. (2017). Modular organization of the brainstem noradrenaline system coordinates opposing learning states. Nat. Neurosci. *20*, 1602–1611.

Valentino, R.J., and Bangasser, D.A. (2016). Sex-biased cellular signaling: molecular basis for sex differences in neuropsychiatric diseases. Dialogues Clin. Neurosci. *18*, 385–393.

Valentino, R.J., Reyes, B., Van Bockstaele, E., and Bangasser, D. (2012). Molecular and cellular sex differences at the intersection of stress and arousal. Neuropharmacology *62*, 13–20.

Weirauch, M.T., Yang, A., Albu, M., Cote, A.G., Montenegro-Montero, A., Drewe, P., Najafabadi, H.S., Lambert, S.A., Mann, I., Cook, K., et al. (2014). Determination and inference of eukaryotic transcription factor sequence specificity. Cell *158*, 1431–1443.

Wright, C.L., Burks, S.R., and McCarthy, M.M. (2008). Identification of prostaglandin E2 receptors mediating perinatal masculinization of adult sex behavior and neuroanatomical correlates. Dev. Neurobiol. *68*, 1406–1419.

Cell Reports, Volume *23*

Supplemental Information

Molecular and Functional Sex Differences of Noradrenergic Neurons in the Mouse Locus Coeruleus

Bernard Mulvey, Dionnet L. Bhatti, Sandeep Gyawali, Allison M. Lake, Skirmantas Kriaucionis, Christopher P. Ford, Michael R. Bruchas, Nathaniel Heintz, and Joseph D. Dougherty

Supplemental Material

Included contents:

Figs. S1 to S5 and legends
Table S2 and legend
Supplemental Experimental Procedures
Supplemental References

See also:

Table S1 (separate .xls file with 9 sheets: 1a-1k)
Table S3 (separate .xls file with 1 sheet)

Supplemental Figures S1-S5: (*beginning on next page*)

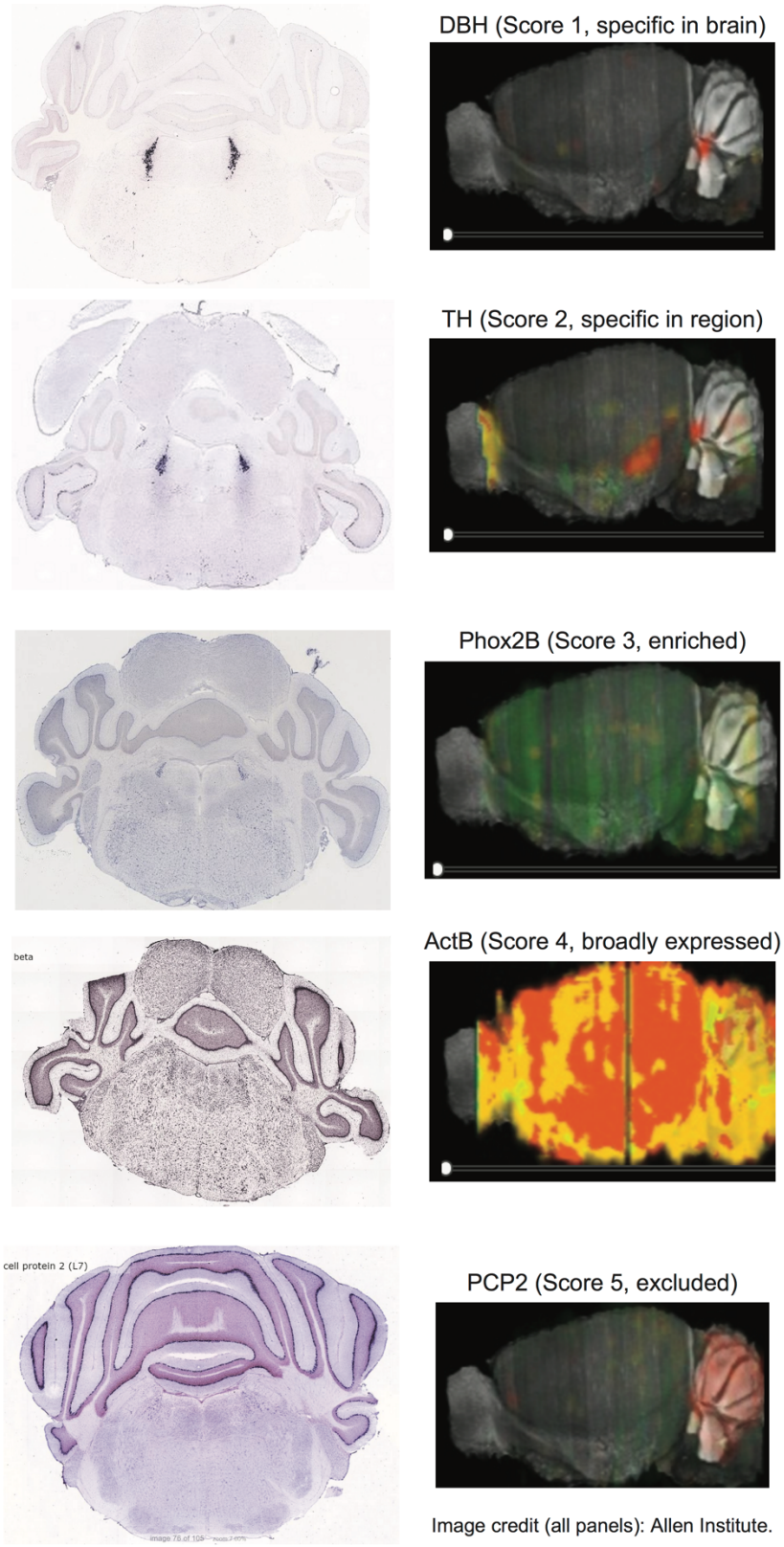

Fig. S1: Examples of Allen Brain Atlas In Situ Hybridizations scored 1-5. Related to Figure 2. Images from Allen Brain Atlas for examples of *in situ* hybridizations that would score a 1-5, respectively. Images of whole sections stitched from higher magnification images.

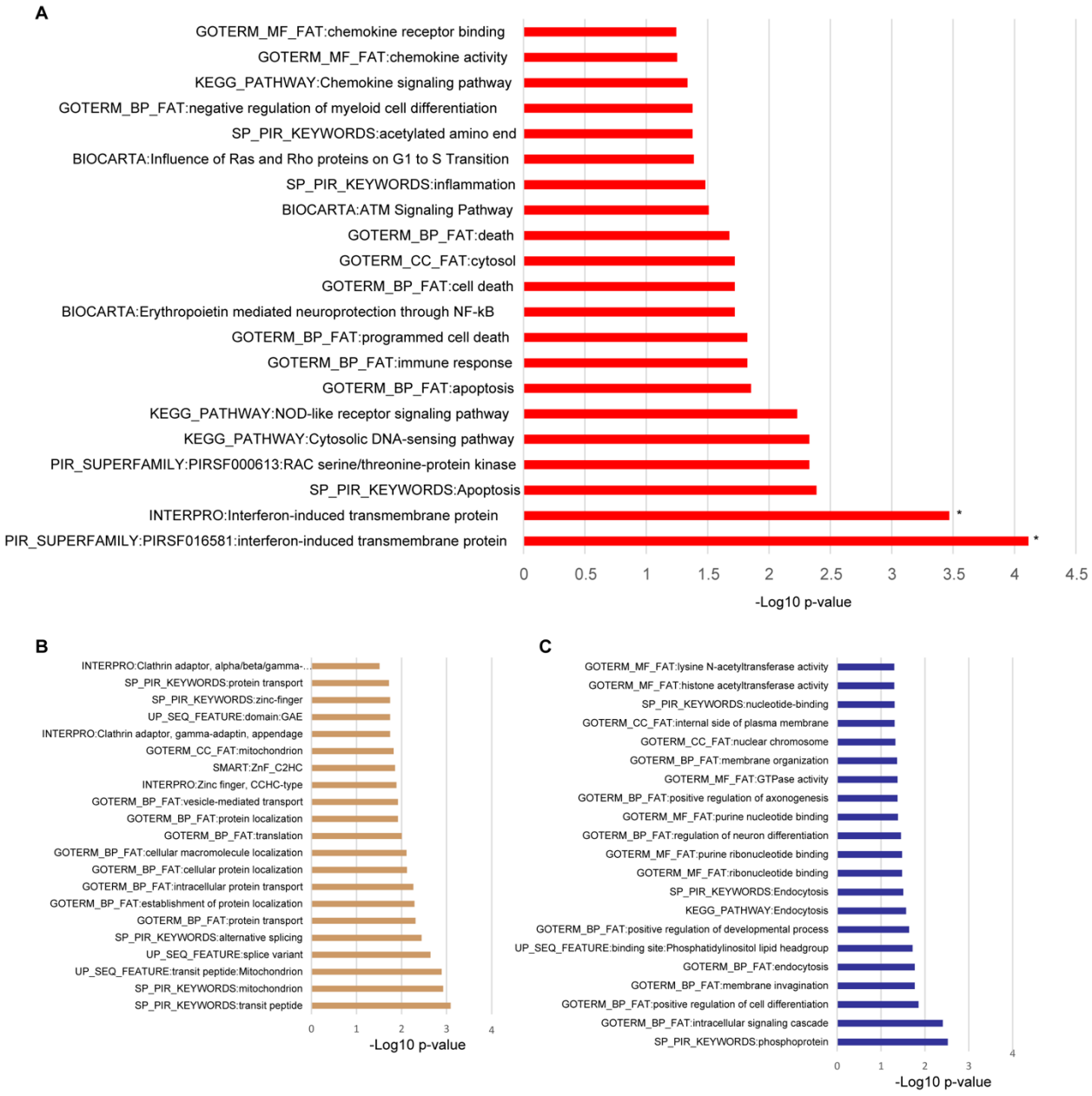

Figure S2: Pathway analysis of transcripts altered in hindbrain by LPS and of sex-differentially expressed transcripts in noradrenergic neurons. Related to Figure 3. A) A pathway analysis using DAVID reveals the hindbrain showed a significant increase of interferon related gene expression, and trends in a variety of chemokine and inflammatory pathways. B,C) An exploratory pathway analysis using DAVID illustrates the trends in male and female noradrenergic gene lists (*-Log10 p-values. No p<0.05 after Benjamini-Hochberg correction for multiple testing).* Though no individual pathway survived correction for multiple testing, the trend towards more mitochondrial genes and vesicular transport transcripts in female neurons may suggest they have slightly higher metabolic demands. Male neurons had slightly more nuclear factors, driven by transcription factors such as *Atrx1*, *Mtf1* and *Pbx1*.

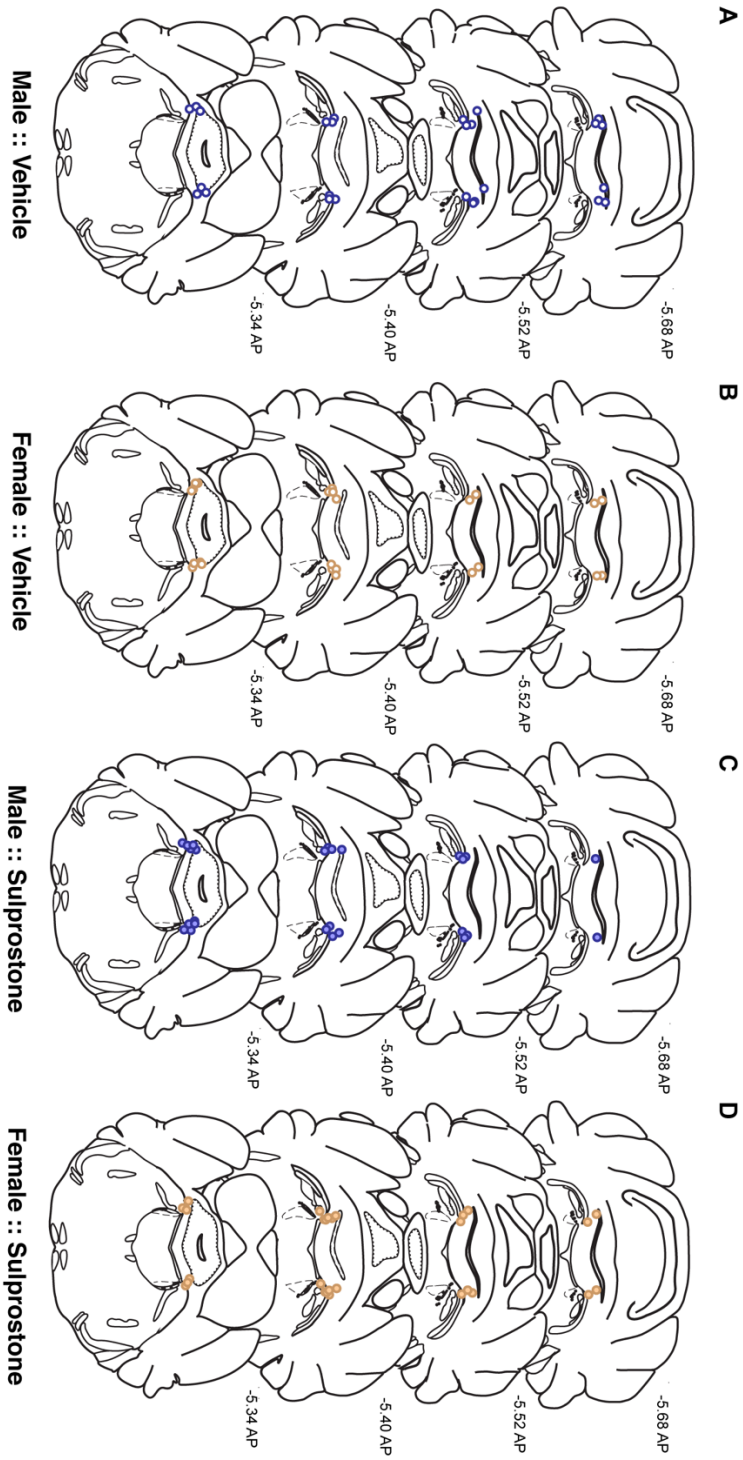

Figure S3: Map of LC cannula placements from post-mortem brain tissue. Related to Experimental Procedures. Tissue from all mice cannulated and given sulprostone or vehicle was sliced, and the deepest point of the two cannula tracks was noted for each mouse. These points are collectively mapped here for mice across all conditions. If cannulae were not in the target area, the mice/tissue were excluded from behavioral analysis, c-FOS quantification, and this diagram. Anatomy is shown in the coronal plane with mm along anterior-posterior (AP) axis;

dotted lines outline location of the LC. Circle outlines: blue = male, orange = female; fill color: purple = sulprostone-treated, empty/white = vehicle-treated.

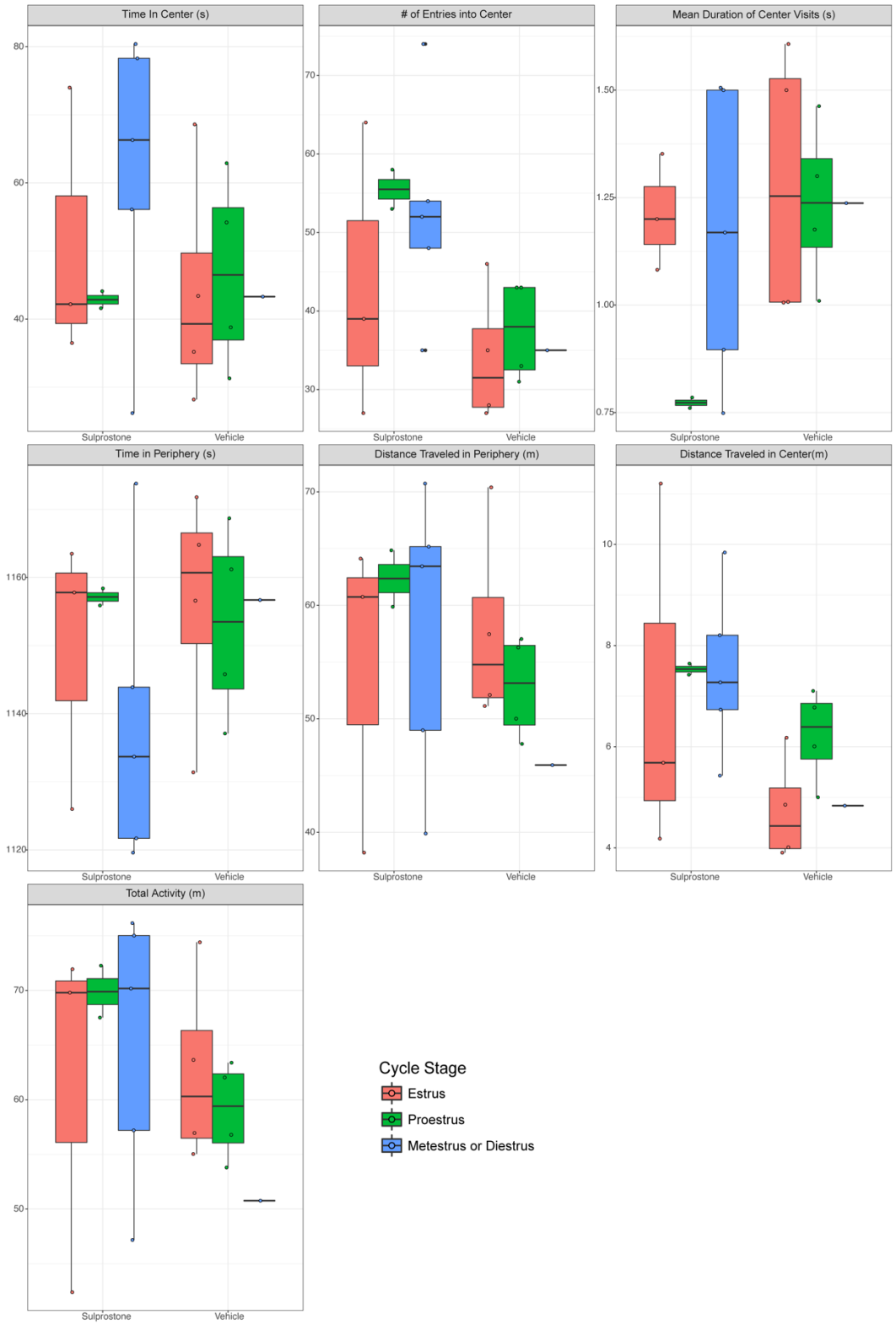

Figure S4: OFT data by estrus stage from one cohort of sulprostone-behavior mice. Related to Figure 4. Boxplots for seven OFT measures in counts, meters (m), or seconds (s) from females in a cohort of sulprostone-behavior mice with estrus staging data. Bottom and top of boxes represent 25th and 75th percentiles, respectively;

line inside the box represents the median (50th percentile), and individual points represent outliers. Metestrus and diestrus were combined per (Silva et al., 2016).

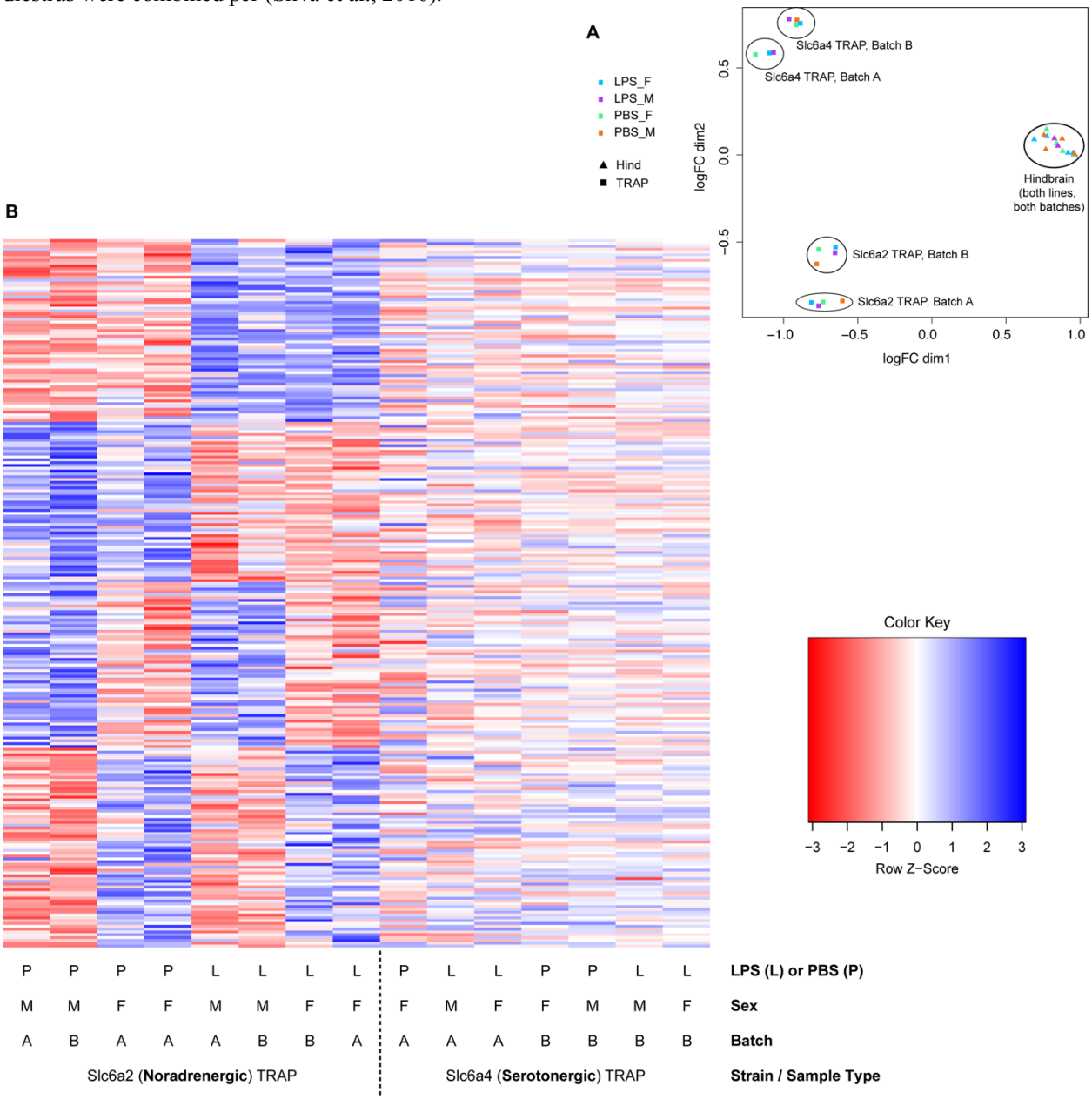

Figure S5: Multidimensional scaling (MDS) and heatmaps illustrate the clustering of samples and gene sets. Related to Figures 1-3 and Experimental Procedures. A) Hierarchical clustering confirms the expected segregation of samples by cell/sample type (*Slc6a2* vs. *Slc6a4* vs. hindbrain, or TRAP vs. hindbrain), and show a degree of batch effects, guiding the analytical strategies employed. B) Clustering genes that were DE between at least one comparison in the *Slc6a2* TRAP samples (i.e., comparing expression between sexes or between LPS/PBS conditions) illustrates the presence of distinct LPS-and sex-dependent DEG sets in noradrenergic neurons. The adjacent *Slc6a4* samples illustrate that sex and LPS do not affect these genes in serotonergic neurons in an analogous manner.

Motif	Total # motif occurrences found	# of unique sequences matching	E-value	Chi-sq p-value (vs. 1,000 random)	Select TFBS Predictions (TomTom)	Sequence
Female LC-Enriched TSS regions						
Fz4	26	26 / 77	1.7E-58	4.59E-03	NR4A2, NR2F6, OTX2	
Fz9**	19	19 / 77	2.7E-24	3.60E-11	(None)	
Fz10	13	13 / 77	3.4E-21	0.5518	OTX2	
Fa4	37	22 / 77	8.0E-97	0.1426	OTX2	
Fa10**	22	17 / 77	1.1E-41	8.28E-13	FOS, FOS::JUN, TBX1, MAZ	
Fa12**	31	19 / 77	6.3E-63	5.43E-07	(None)	
Male LC-Enriched TSS regions						
Mz1	15	15 / 70	1.5E-46	0.5645	(None)	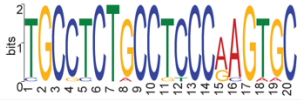
Mz2**	20	20 / 70	1.5E-19	4.50E-04	MTF1, OTX2	
Ma3*	31	24 / 70	2.1E-104	5.17E-03	NR2F6, OTX2	
Ma4*	23	18 / 70	3.1E-61	0.0198	OTX2	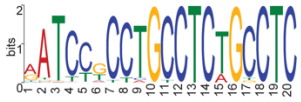
Mvf1	13	13 / 70	1.0E-44	1.00	Let-7, NR2F6, MAZ	
Mvf3	11	11 / 70	2.1E-07	0.1531	(None)	

Table S2: Motifs discovered in conserved, noncoding regions near sex-DEGs. Related to Experimental Procedures.

Motif: Refers to the sex, algorithm (allowing ≤ 1 or ≥ 1 motif occurrence per query sequence) and the result # in the MEME output. *Total # motif occurrences found:* total number of significant matches for the motif. *# Unique sequences matching:* the number of queried sequences with ≥ 1 motif match out of the total number of sequences queried. *E-value*: a MEME measure of probability compared to a shuffled version of the input sequences. *Chi-sq p value*: from comparative abundance of the identified motif in 1,000 randomly selected, protein-coding gene regions subjected to the same masking paradigm. *Select TFBS predictions*: TFBSes identified using TomTom with previously described expression in neural cell types and of functional and/or cell type relevance to the LC. *Sequence*: the position-weight matrix (PWM) given in the MEME results.

Supplemental Experimental Procedures

Animal Research Statement

All procedures involving animals were approved by the Institutional Animal Care and Use Committees of Rockefeller University, Case Western Reserve University, and Washington University in St. Louis.

Generation of LC TRAP mice and selection of an LC-specific TRAP mouse line. We initially modified BACs to be controlled by the promoters of either of two genes with LC-specific expression: Dopamine Beta Hydroxylase (*Dbh,* BAC RP23-354N13)*,* involved in the synthesis of NE (*16*), and the NE reuptake transporter (*Slc6a2,* RP23-109O23) (*17*). BACs were modified as described (Doyle et al., 2008) to insert the TRAP transgene (EGFP/Rpl10a) at the translation start site of the relevant gene. Successful modification was confirmed with Southern blot, and the absence of gross rearrangements in the BACs was verified by BAC fingerprinting and pulse field gel. Modified BAC DNA was purified with CsCl gradient centrifugation, dialyzed into injection buffer, and injected into FVB mouse eggs. Eggs were transplanted into pseudo-pregnant Swiss Webster dams; tail tips of the resultant pups were PCR genotyped for EGFP to identify founders. Founders were crossed to C57/BL6J wildtype mice, whose F1 progeny were genotyped and processed for anatomy as described below. Multiple founder lines were evaluated for EGFP expression; lines from both *Dbh* and *Slc6a2* constructs showed EGFP/Rpl10a expression in the LC and other noradrenergic populations. The lines for *Slc6a2* consistently demonstrated more robust EGFP/Rpl10a expression—as described in the main text's results section and **Figure 1**—and were thus selected for complete anatomical and biochemical evaluation. Two of the *Slc6a2* founders were used for initial transcriptional profiling (these lines were delegated B6;FVB-Tg (*Slc6a2*-EGFP/Rpl10a)JD1537$^{Jdd/J}$ and B6;FVB-Tg (*Slc6a2*-EGFP/Rpl10a)JD1538$^{Jdd/J}$) (**Figure 1E**, **2A**). The line JD1538 was further used to contrast transcriptional profiles of LC under different fixed and environmental conditions (sex and LPS injection) (**Figure 3**).

Immunofluorescence microscopy. Mice were sacrificed then perfused with phosphate buffered saline (PBS) followed by 4% paraformaldehyde in PBS. Brains were dissected, cryoprotected in 30% sucrose PBS solution, frozen, and sectioned serially on a Leica cryostat into PBS with 0.1% sodium azide for storage at 4°C. Floating sections were incubated at room temperature for 30 minutes in a blocking buffer of 5% normal donkey serum and 0.25% Triton in PBS followed by overnight incubation with primary antibodies in blocking buffer. Sections were washed 3 times with PBS, then incubated for 60-90 minutes with appropriate Alexa fluorophore-conjugated secondary antibodies and nuclear dye (DAPI or TOPO-3-Iodide, *Life Technologies*). Images were acquired on a LSM 510 Zeiss confocal microscope or a Perkin Elmer UltraView Vox spinning disk confocal via a Zeiss Axiovert microscope. Antibodies used are described in **Table S1j**.

Immunohistochemistry. Mice were processed as above. For anti-GFP DAB immunohistochemistry, brains were processed utilizing multibrain technology by Neuroscience Associates (*Knoxville, TN)* as described (Doyle et al., 2008), using a custom goat anti-GFP antibody and a Nickel enhanced DAB substrate for HRP. Sections were digitized with a Zeiss Axioskop2 using customized macros.

In-situ *hybridization (ISH) for detection of Calcr mRNA*. Two adult (P>60) C57BL/6J male littermates and one P35 male FVB-Ant mouse were sacrificed by CO_2 asphyxiation. Brains were transferred to cryoprotectant, and stored at -80°C for <4 weeks. 20µm cryosections were cut and directly mounted onto slides for ISH. The antisense *Calcr* probe region was selected to complement a constitutive exon. The probe was amplified by PCR with primers containing an appropriately-oriented T7 polymerase promoter, and probes were subsequently synthesized by *in vitro* transcription (per mfg. instructions) using T7 polymerase (*Promega #P2075*) and Digoxigenin RNA Labeling Mix (*Roche #11277073910*). For ISH, slides were incubated in 4% paraformaldehyde for 10min to fix tissue. Probe was hybridized to slides in a humid chamber at 68°C overnight and washed. Alkaline phosphatase-coupled anti-digoxigenin antibodies (**Table S1j**) were used for detection (4°C overnight incubation), followed by staining with NBT and BCIP, resulting in black staining by alkaline phosphatase. Primers for the *Calcr* probe were: 5' GCCAGTGGACGCAGTTCAAGATCCAGTGG 3' and 5' **gcacgTAATACGAC-TCACTATAG**GCCTGCTTTCCTACGAACACAGTCATCTCAGTCC 3' (in bold lowercase: bases added to end to allow room for T7 association, per mfg. instructions; in bold uppercase, the T7 promoter).

TRAP for initial description of LC. Replicate pools of five mixed sex adult mice from each of the *Slc6a2* lines were sacrificed. Brains were removed and transferred to ice-cold dissection buffer containing cycloheximide for collection of hindbrain posterior to the pontine/hypothalamic junction (discarding the cerebellum). TRAP was conducted as described (Doyle et al., 2008). Briefly, each pooled sample of hindbrains was homogenized in buffer

(10 mM HEPES [pH 7.4], 150 mM KCl, 5 mM $MgCl_2$, 0.5 mM dithiothreitol, 100 µg/ml cycloheximide, protease inhibitors, and recombinant RNase inhibitors) using a glass teflon homogenizer on ice. Nuclei and debris were removed with centrifugation at 2000 x *g* for 10 min at 4°C. DHPC (Avanti, Alabastar, AL) and NP-40 (Ipgal-ca630, Sigma, St Louis, MO) were added to the supernatant (final concentrations of 30mM and 1%, respectively) and incubated on ice for 5 minutes. This supernatant was centrifuged at 20,000 x *g* for 15 minutes at 4°C, and pellet was discarded. Protein G-coated magnetic beads (Invitrogen/Life Technologies, Grand Island, NY), conjugated to a mix of two monoclonal anti-GFP antibodies (Doyle et al., 2008), and incubated with supernatant by rotation for 30 minutes at 4°C. Beads were washed three times with high salt wash buffer (10 mM HEPES [pH 7.4], 350 mM KCl, 5 mM $MgCl_2$, 1% NP-40, 0.5 mM dithiothreitol, and 100 µg/ml cycloheximide). RNA was purified from ribosomes using Trizol (Invitrogen), followed by DNAse treatment, further purification, and concentration with RNeasy MinElute columns (*Qiagen, Hilden, Germany*) according to the manufacturers' protocols. RNA was also harvested in parallel from each unbound fraction of affinity purification as a measure of total hindbrain RNA. RNA concentration of all samples was measured with Nanodrop spectrophotometer and integrity (RIN>8) was confirmed with PicoChips on the Agilent BioAnalyzer.

Each RNA sample was amplified with the Affymetrix Two-Cycle amplification kit per manufacturer's instructions. Quality of labeled aRNA was assessed with Bioanalyzer. aRNAs from immunoprecipitated ribosomes and total tissue were hybridized to separate Affymetrix Mouse Genome 430 2.0 arrays and scanned following manufacturer protocols. Raw data are available from the Gene Expression Omnibus (GEO): **GSE100005.**

Data were analyzed using the Bioconductor module within the R programming language. Data were normalized as described (Dougherty et al., 2010). Briefly, GCRMA was used to normalize within replicates, and to biotinylated spike in probes (green dots, **Figure 1F**) between conditions. Fold change, Specificity Index (SI) and pSI were calculated for all genes with expression above non-specific background, and >50 arbitrary fluorescent units, as described (Dougherty et al., 2010). The threshold to identify genes expressed above background was conservatively set at the mean plus 2 standard deviations of the fold change of negative control transcripts comparing the TRAP samples to hindbrain mRNA (**Figure 1F**, red dots). Genes with expression below this level may or may not be found in LC neurons. To identify transcripts enriched in LC neurons compared to hindbrain RNA, we utilized the empirical Bayesian statistic with FDR correction within the *l*imma package. Positive control transcripts plotted in **Figure 1** include genes with known specificity and functionality in LC: *Th (Austin et al., 1990; Bacopoulos and Bhatnagar, 1977), Ddc* (Weihe et al., 2006), *Maoa (Hasegawa et al., 1999)*, *Dbh* (Swanson and Hartman, 1975), *Slc18a2* (Weihe et al., 2006)*, Slc6a2*, *Gal, GalR1* (Melander et al., 1986), and *Phox2a* (Morin et al., 1997). We used the pSI algorithm with default settings to compare the LC expression profile with other mouse brain cell populations characterized by TRAP (Dalal et al., 2013; Dougherty et al., 2013; Doyle et al., 2008; Görlich et al., 2013; Xu et al., 2014). Cell types included in this analysis are listed in **Figure 1G**. Hierarchical clustering across cell types was conducted in R utilizing expression values from genes with pSI <0.01 in any cell type. Finally, Gene Ontologies analysis throughout the manuscript was conducted with the DAVID interface's Functional Annotation Chart tool (Dennis et al., 2003).

Single animal TRAP for sex-differential and LPS-responsive gene expression. Four adult male and four adult female mice from each of the bacTRAP lines (B6;FVB-Tg (*Slc6a4*-EGFP/Rpl10a)JD60$^{Htz/J}$ (Dougherty et al., 2013), and B6;FVB-Tg (*Slc6a2*-EGFP/Rpl10a)JD1538$^{Jdd/J}$) were surgically implanted with peritoneal G2 E-Mitter Transponders (*Phillips Respironics*), then single-housed for 48 hours to allow continuous telemetric monitoring of temperature and activity using the Vital View software and ER-4000 Energizer Receivers. Housing was maintained at 30°C (thermoneutral for a mouse) to permit induction of fever (Chai et al., 1996; Gordon, 1993; Kozak et al., 1998; Leon, 2002). On the day of the experiment, mice were injected at 07:30 AM intraperitoneally with 100 ug/kg of LPS (Sigma 0111:B4) or vehicle (sterile PBS) and monitored for lethargy and induction of fever with telemetery. Pilot experiments in a separate cohort established that fever peaked around 14:00. Experimental mice were euthanized at 14:00-14:30, at which point mice displayed substantial lethargy and a mean fever of 2.175°C ± 1.18 (SD) above preceding minimal body temperature. Hindbrains were dissected and processed for TRAP as described (Heiman et al., 2014). RNA quality was checked as above and quantified with Ribogreen assay. 3-7 ng per sample were amplified with Nugen Ovation PicoSL and hybridized to Illumina Mouse WG6 microarrays. Samples were handled and hybridized in two batches counterbalanced for mouse line, sex, and LPS exposure. Data were analyzed using Bioconductor/R. Examination of distribution of expression levels led to the exclusion of one *Slc6a4* TRAP sample and two hindbrain samples for poor hybridization. Remaining TRAP and hindbrain samples were separately normalized using the lumi package. Appropriate clustering of replicates was confirmed with multidimensional

scaling (MDS) (**Figure S5**). TRAP samples were again compared to hindbrain mRNAs, which confirmed TRAP enrichment of markers for each respective cell type. Only genes with TRAP/hindbrain expression above glial background (Dougherty et al., 2010) (>0.85 here), and absolute expression >200 fluorescent units were included for downstream expression comparisons (sex or LPS/PBS). For each mouse line, probes were defined as differentially expressed if p<.05 on a paired T-test (pairing by experimental batch and covariate) and Log2 change was +/- .585 (1.5 fold) across 3 of 4 paired comparisons. For balance purposes, the remaining replicate was used twice to replace the low quality excluded *Slc6a4* TRAP sample. Results of these analyses are in **Table S1c-S1g**.

Our paired T-test approach accounted for batch effects by design and restricted our candidate DEGs to those with a fold-difference in expression of >1.5 across ≥3 of 4 paired comparisons. This achieved our primary goal of identifying high-confidence cell-type specific markers and functional targets like *Ptger3*.

However, to identify DEGs less stringently (simply a significant *average* fold-change of 1.5), and to sidestep re-using samples in paired t-tests, we also performed intercept-free linear modeling analysis in R using the *limma* package on the same microarray data from the *Slc6a2*-LPS and *Slc6a4*-LPS experiments. The model was implemented using the following formula:

design <- model.matrix(~0+group+batch)

Where the group variable was coded as follows for the *Slc6a2* model (and analogously for the *Slc6a4* model):

sample_id	cell_type	treat	trap	sex	Batch	group
A2.P.F.IP_A1	SLC6A2	PBS	T	F	B	PBS_F_T
A2.P.F.IP_C3	SLC6A2	PBS	T	F	A	PBS_F_T
A2.P.M.IP_A3	SLC6A2	PBS	T	M	B	PBS_M_T
A2.P.M.IP_A5	SLC6A2	PBS	T	M	A	PBS_M_T
A2.L.F.IP_A2	SLC6A2	LPS	T	F	B	LPS_F_T
A2.L.F.IP_A6	SLC6A2	LPS	T	F	A	LPS_F_T
A2.L.M.IP_A4	SLC6A2	LPS	T	M	A	LPS_M_T
A2.L.M.IP_C1	SLC6A2	LPS	T	M	B	LPS_M_T
A2.P.F.PRE_D6	SLC6A2	PBS	P	F	A	PBS_F_P
A2.P.F.UB_D1	SLC6A2	PBS	P	F	B	PBS_F_P
A2.P.M.PRE_D4	SLC6A2	PBS	P	M	A	PBS_M_P
A2.P.M.UB_D3	SLC6A2	PBS	P	M	B	PBS_M_P
A2.L.F.PRE_D5	SLC6A2	LPS	P	F	A	LPS_F_P
A2.L.F.UB_D2	SLC6A2	LPS	P	F	B	LPS_F_P
A2.L.M.UB_F1	SLC6A2	LPS	P	M	B	LPS_M_P

The desired comparisons were made between groups using the following contrasts:

MvF_Trap = (PBS_M_T + LPS_M_T)/2 - (PBS_F_T + LPS_F_T)/2
LPSvPBS_Trap = (LPS_M_T + LPS_F_T)/2 - (PBS_M_T + PBS_F_T)/2
MvF_Pre = (PBS_M_P + LPS_M_P)/2 - (PBS_F_P + LPS_F_P)/2
LPSvPBS_Pre = (LPS_M_P + LPS_F_P)/2 - (PBS_M_P + PBS_F_P)/2
TrapvPre_M = (PBS_M_T + LPS_M_T)/2 - (PBS_M_P + LPS_M_P)/2
TrapvPre_F = (PBS_F_T + LPS_F_T)/2 - (PBS_F_P + LPS_F_P)/2
TrapvPre_LPS = (LPS_M_T + LPS_F_T)/2 - (LPS_M_P + LPS_F_P)/2
TrapvPre_PBS = (PBS_M_T + PBS_F_T)/2 - (PBS_M_P + PBS_F_P)/2

Note that for assessing main effects of sex or LPS, the available *n* of LC TRAP samples was 4. We did not examine interaction effects for lack of statistical power (*n=2* for the cross-comparison). For *Slc6a2* mice, this analysis

revealed 277 genes with sex-differential upregulation in male *Slc6a2* cells and 304 genes with sex-differential upregulation in female *Slc6a2* cells (including >85% of those from analysis above). This was still substantially higher than the sex-differentially upregulated gene sets from *Slc6a4* mice (15 genes in male, 15 genes in female). Resulting *p*-values from the latter analytical approach for genes passing differential expression criteria of the former approach are included in **Table S1c-S1g**. Fold changes and *p*-values from the *limma* analysis for the entire the entire array probeset are in **Table S3**.

Motif Analysis of peri-TSS Sequences of Sex-DEGs in LC: sequence acquisition and exon masking. For each sex-differentially expressed gene identified in the LC (**Table S1f,g**), mm10 genomic coordinates covering 10kb 5' and 10kb 3' to the canonical TSS were acquired from UCSC genome browser. For genes with multiple transcripts, the TSS of the longest transcript was selected. To perform motif discovery strictly within noncoding DNA sequences, the coordinates of all exon sequences in each range were acquired from UCSC. The mm10 genome was hard-masked (e.g., C->N) within all exon coordinates using *bedtools maskfasta*. The FASTA sequences for the 20kb regions were then extracted from the exon-masked genome using *bedtools getfasta*.

Conservation scoring and masking prior to MEME. For each base over 20kb regions, PhyloP scores—quantifying sequence conservation among placental mammals—were retrieved from UCSC**.** The threshold for defining conservation was a PhyloP score of 0.28, determined by counting the number of bases exceeding a score in steps of 0.01 and finding the step giving the greatest decrease in number of suprathreshold bases; this score corresponded to approximately 25% of input bases. Finally, to smooth the data, we used a "sliding mean" algorithm, acquiring the mean PhyloP score 15bp upstream and 15bp downstream of each base, with a step size of 1. Bases falling within ≥ 1 31bp window with a suprathreshold mean conservation score were retained; all others were hard-masked within the existing exon-masked sequences.

MEME analysis. Masked sequence sets for the male-enriched and female-enriched genes were then submitted to MEME (Bailey et al., 2015) for *de novo* motif analysis for motifs ranging 8-20bp in size. Two analyses were performed: one using the –zoops setting, which assumes and detects no more than one instance of a motif in each input sequence, and another using the –anr setting, which allows detection of multiple repeats of a motif within a given input sequence. The former allows us to detect how many sequences contain a given motif, while the latter allows us to detect how many total occurrences of a motif were found. MEME returns E-values, a built-in calculation of the likelihood of a motif occurring as many times as observed compared to a MEME-generated scrambled version of the input sequence. In the third "discriminative" analysis, one sex's sequence set was submitted as input and the other's as control, wherein E-scores represent the comparison between the input and "control" set, as opposed to input vs. scrambled. "Discriminative mode" in MEME only allows use of the –zoops algorithm; therefore, -anr data could not be collected for the direct sequence comparisons. For identification of putative TF binding sites represented by these motifs, we submitted the motifs from MEME to another MEME suite tool, TomTom, comparing those motifs to known murine and vertebrate TF binding sites (Kulakovskiy et al., 2018; Mathelier et al., 2016; Weirauch et al., 2014).

Chi-square analysis of motif-containing genes in LC sex-enriched sets vs background. To assess whether the abundance of these motifs near sex-differentially expressed LC transcripts differed from the genome on the whole, 1000 random protein-coding TSSes were selected for generation and masking of analogous 20kb windows using the same pipeline. These sequences were searched for matches to the discovered motifs using FIMO at the same *p* cutoff for a "match" used during motif discovery. The number of unique genes in the background set containing ≥ 1 occurrence of the motif was then counted and compared to the sex-differential gene set using chi-square analysis, followed by Benjamani-Hochberg correction for twelve tests (one per motif).

Electrophysiology of LC neurons exposed to PTGER3 agonist/antagonist. Horizontal brain slices were obtained from deeply anesthetized 6-7 week old male and female C57/BL6J mice (*Jackson Laboratories*) containing the LC (240 μM), as described (Courtney and Ford, 2014). Briefly, brain slices were cut using a Vibratome (Leica) in warm (~30°C) artificial cerebral-spinal fluid (aCSF) solution containing (in mM): 126 NaCl, 2.5 KCl, 1.2 $MgCl_2$, 2.5 $CaCl_2$, 1.2 NaH_2PO_4, 21.4 $NaHCO_3$, and 11.1 D-glucose bubbled with 95% O_2 and 5% CO_2. Slices were incubated at 35°C for at least 45 minutes prior to use. MK-801 (10 μM) was included during the incubation to block NMDA receptors. Following incubation, slices were transferred to a recording chamber and constantly perfused at 2 ml/min with oxygenated aCSF warmed to 34 ± 2°C. Slices were visualized with a BX51WI microscope (Olympus) with custom-built infrared gradient contrast optics.

Whole-cell recordings were made using an Axopatch 200B amplifier (*Molecular Devices*). Patch pipettes (2.0-2.5 MΩ) were pulled from borosilicate glass (*World Precision Instruments*). For voltage clamp experiments the pipette internal solution contained (in mM): 115 K-methylsulphate, 20 NaCl, 1.5 $MgCl_2$, 10 K-HEPES, 10 BAPTA-tetrapotassium, 2 ATP, 0.3 GTP, and 6 sodium phosphocreatine; pH 7.4; 275 mOsm. LC neurons were held at a voltage of -60 mV. No series resistance compensation was used, and cells were discarded if their series resistance exceeded 15 MΩ. For current clamp experiments the pipette internal solution contained (in mM): 135 D-gluconate (K), 10 HEPES (K), 0.1 $CaCl_2$, 2 $MgCl_2$, 0.1 EGTA, 1 mg/mL ATP, 0.1 mg/mL GTP, and 1.5 mg/mL phosphocreatine, pH 7.4, 275 mOsm. Liquid junction potentials were not corrected. All recordings were acquired using an ITC-18 interface (*Instrutech*) and Axograph X (*Axograph Scientific*) at 5 kHz and filtered to 2 kHz. For presentation, long chart recordings were made using a Powerlab 4/20 and LabChart (*AD Instruments*). Data was sampled for presentation at 400 Hz. The LC was identified by its location between the mesencephalic tract motor neurons and the 4th ventricle and neurons were identified by a capacitance > 40 pF, an input resistance < 100 MΩ, and a tonic firing rate of 0.5 – 4 Hz. Examination of the current-voltage relationship of the sulprostone-evoked outward current revealed inward rectification and a hyperpolarized reversal potential (-120 mV).

Stereotaxic cannulation of LC. Adult male and female C57BL/6J mice (8-10 weeks) were group-housed, given *ad libitum* access to food pellets and water and maintained on a 12/12 hour light:dark cycle (lights on at 6:00 AM). For surgery, mice were anesthetized in an induction chamber (4% isoflurane), then placed in a stereotaxic frame (*Kopf Instruments, Model 1900*) where they were maintained at 1-2% isoflurane. We performed craniotomies for insertion of two anchor screws and bilateral cannulae (*PlasticsOne, Inc*.). Cannulae were implanted above the LC (AP -5.45, ML +/-1.00, DV -3.00 mm relative to Bregma). Cannulae and anchor screws were then affixed to the skull using dental cement. Mice were allowed to recover for 7-9 days prior to behavioral testing. Animals were also habituated to handling and connection to pharmacological tubing for 3 consecutive days prior to behavioral testing.

Sulprostone and vehicle preparation for intracranial infusion. A 10.7mM (5mg/mL) stock solution of sulprostone in 200uL methyl acetate (*Tocris*) was diluted with an additional 800uL methyl acetate (*Sigma Aldrich*) to achieve a stock concentration of 1mg/mL. 1.12uL of this solution was then added to 12mL aCSF, achieving a final concentration of 200nM (the same concentration applied to *ex vivo* LC slices). 1.12uL of methyl acetate was added to 12mL aCSF for the vehicle-only controls.

Stress-induced anxiety behavioral paradigm. Mice were intracranially infused via bilateral cannulae with either sulprostone (0.4 µL per side, delivering 3.72pg sulprostone per side for drug condition) or its vehicle at a rate of 0.2 µL/min. Immediately following infusion, all mice were restrained for 30 minutes in 50 mL plastic conical tubes with drilled holes permitting air circulation and allowing the tail to extend beyond the tube (adapted from (McCall et al., 2015)). Immediately following restraint stress, animals were transferred to the open field for a 20-minute test. The open field testing (OFT) was performed in a rectangular enclosure 59x39 cm within a sound attenuated enclosure with lighting measured and maintained at ~25 lux. The open field was cleaned with 70% ethanol between each trial. Mice were returned to their home cage for 50 minutes after OFT; 10 minutes later (60min after the end of OFT), isoflurane anesthesia was administered prior to paraformaldehyde perfusion and brain dissection (as previously described). For the no-drug (stress vs. no-stress only, **Figure 4E-4H**), no surgeries or intracranial infusions were performed, and this same protocol was used beginning with the 30 minutes of restraint. Anymaze was used for video recording of animal movements for center and periphery analysis. The center zone was defined as a concentric rectangle comprised of 50% the total area of the OFT arena. Time and frequency in the center was used as a measure of anxiety-like behavior. Cannula placement was confirmed by cryostat sectioning of perfused brains to determine mice for inclusion in the final behavioral and c-FOS analyses.

c-FOS quantification in LC following sulprostone/vehicle, restraint, and OFT. Following behavior, perfusion, and slicing, 40µm sections of brain containing LC were subjected to immunohistochemistry for phospho-Ser32 c-Fos and TH (n=5 vehicle treated males, 5 vehicle-treated females, 4 sulprostone-treated males, 6 sulprostone-treated females; see methods described under *Immunohistochemistry*). Antibodies are described in **Table S1j**. All sections were imaged on a Zeiss AxioScan.Z1 microscope (Karl Zeiss, Germany). Gain, light intensity, and exposure time were identical for all prepared microscope slides. All images were processed with the same settings using ImageJ: background was first subtracted from the images, ROIs were made around the LC as determined by TH expression, and average pixel intensity was measured. Additionally, the number of Fos-expressing and TH-expressing cells were counted manually by an experimenter blind to treatment groups.

Estrous staging of female mice after OFT paradigm. In order to assess whether estrous stages and their corresponding hormonal milieus influenced baseline or sulprostone-moderated behaviors, vaginal cytology was

performed after female mice were anesthetized, but before perfusion began. Cytology was performed using 100uL H2O to perform vaginal lavage, followed by cresyl violet staining of the dried smear as previously described (McLean et al., 2012). Estrous stage was assessed as proestrous, estrous, metestrous, or diestrous by light microscopy based on cell types and structures (Byers et al., 2012; McLean et al., 2012).

Supplemental References:

Austin, M.C., Cottingham, S.L., Paul, S.M., and Crawley, J.N. (1990). Tyrosine hydroxylase and galanin mRNA levels in locus coeruleus neurons are increased following reserpine administration. Synapse *6*, 351–357.

Bacopoulos, N.G., and Bhatnagar, R.K. (1977). Correlation between tyrosine hydroxylase activity and catecholamine concentration or turnover in brain regions. J. Neurochem. *29*, 639–643.

Bailey, T.L., Johnson, J., Grant, C.E., and Noble, W.S. (2015). The MEME Suite. Nucleic Acids Res. *43*, W39–49.

Byers, S.L., Wiles, M.V., Dunn, S.L., and Taft, R.A. (2012). Mouse Estrous Cycle Identification Tool and Images. PLOS ONE *7*, e35538.

Chai, Z., Gatti, S., Toniatti, C., Poli, V., and Bartfai, T. (1996). Interleukin (IL)-6 gene expression in the central nervous system is necessary for fever response to lipopolysaccharide or IL-1 beta: a study on IL-6-deficient mice. J. Exp. Med. *183*, 311–316.

Courtney, N.A., and Ford, C.P. (2014). The Timing of Dopamine- and Noradrenaline-Mediated Transmission Reflects Underlying Differences in the Extent of Spillover and Pooling. J. Neurosci. *34*, 7645–7656.

Dalal, J., Roh, J.H., Maloney, S.E., Akuffo, A., Shah, S., Yuan, H., Wamsley, B., Jones, W.B., Strong, C. de G., Gray, P.A., et al. (2013). Translational profiling of hypocretin neurons identifies candidate molecules for sleep regulation. Genes Dev. *27*, 565–578.

Dennis, G., Sherman, B.T., Hosack, D.A., Yang, J., Gao, W., Lane, H.C., and Lempicki, R.A. (2003). DAVID: Database for Annotation, Visualization, and Integrated Discovery. Genome Biol. *4*, R60.

Dougherty, J.D., Schmidt, E.F., Nakajima, M., and Heintz, N. (2010). Analytical approaches to RNA profiling data for the identification of genes enriched in specific cells. Nucleic Acids Res. *38*, 4218–4230.

Dougherty, J.D., Maloney, S.E., Wozniak, D.F., Rieger, M.A., Sonnenblick, L., Coppola, G., Mahieu, N.G., Zhang, J., Cai, J., Patti, G.J., et al. (2013). The disruption of Celf6, a gene identified by translational profiling of serotonergic neurons, results in autism-related behaviors. J. Neurosci. Off. J. Soc. Neurosci. *33*, 2732–2753.

Doyle, J.P., Dougherty, J.D., Heiman, M., Schmidt, E.F., Stevens, T.R., Ma, G., Bupp, S., Shrestha, P., Shah, R.D., Doughty, M.L., et al. (2008). Application of a Translational Profiling Approach for the Comparative Analysis of CNS Cell Types. Cell *135*, 749–762.

Gordon, C. (1993). Temperature Regulation in Laboratory Rodents (Cambridge University Press).

Görlich, A., Antolin-Fontes, B., Ables, J.L., Frahm, S., Slimak, M.A., Dougherty, J.D., and Ibañez-Tallon, I. (2013). Reexposure to nicotine during withdrawal increases the pacemaking activity of cholinergic habenular neurons. Proc. Natl. Acad. Sci. U. S. A. *110*, 17077–17082.

Hasegawa, Y., Hida, T., and Arai, R. (1999). Noradrenaline-degrading activity of monoamine oxidase is localized in noradrenergic neurons of the locus coeruleus of the rat. Neurosci. Lett. *264*, 61–64.

Heiman, M., Kulicke, R., Fenster, R.J., Greengard, P., and Heintz, N. (2014). Cell type–specific mRNA purification by translating ribosome affinity purification (TRAP). Nat. Protoc. *9*, 1282–1291.

Kozak, W., Kluger, M.J., Soszynski, D., Conn, C.A., Rudolph, K., Leon, L.R., and Zheng, H. (1998). IL-6 and IL-1 beta in fever. Studies using cytokine-deficient (knockout) mice. Ann. N. Y. Acad. Sci. *856*, 33–47.

Kulakovskiy, I.V., Vorontsov, I.E., Yevshin, I.S., Sharipov, R.N., Fedorova, A.D., Rumynskiy, E.I., Medvedeva, Y.A., Magana-Mora, A., Bajic, V.B., Papatsenko, D.A., et al. (2018). HOCOMOCO: towards a complete collection of transcription factor binding models for human and mouse via large-scale ChIP-Seq analysis. Nucleic Acids Res. *46*, D252–D259.

Leon, L.R. (2002). Invited Review: Cytokine regulation of fever: studies using gene knockout mice. J. Appl. Physiol. *92*, 2648–2655.

Mathelier, A., Fornes, O., Arenillas, D.J., Chen, C.-Y., Denay, G., Lee, J., Shi, W., Shyr, C., Tan, G., Worsley-Hunt, R., et al. (2016). JASPAR 2016: a major expansion and update of the open-access database of transcription factor binding profiles. Nucleic Acids Res. *44*, D110-5.

McCall, J.G., Al-Hasani, R., Siuda, E.R., Hong, D.Y., Norris, A.J., Ford, C.P., and Bruchas, M.R. (2015). CRH Engagement of the Locus Coeruleus Noradrenergic System Mediates Stress-Induced Anxiety. Neuron *87*, 605–620.

McLean, A.C., Valenzuela, N., Fai, S., and Bennett, S.A.L. (2012). Performing vaginal lavage, crystal violet staining, and vaginal cytological evaluation for mouse estrous cycle staging identification. J. Vis. Exp. JoVE e4389–e4389.

Melander, T., Hökfelt, T., Rökaeus, A., Cuello, A.C., Oertel, W.H., Verhofstad, A., and Goldstein, M. (1986). Coexistence of galanin-like immunoreactivity with catecholamines, 5-hydroxytryptamine, GABA and neuropeptides in the rat CNS. J. Neurosci. *6*, 3640–3654.

Morin, X., Cremer, H., Hirsch, M.R., Kapur, R.P., Goridis, C., and Brunet, J.F. (1997). Defects in sensory and autonomic ganglia and absence of locus coeruleus in mice deficient for the homeobox gene Phox2a. Neuron *18*, 411–423.

Schroeter, S., Apparsundaram, S., Wiley, R.G., Miner, L.H., Sesack, S.R., and Blakely, R.D. (2000). Immunolocalization of the cocaine- and antidepressant-sensitive l-norepinephrine transporter. J. Comp. Neurol. *420*, 211–232.

Silva, A.F., Sousa, D.S., Medeiros, A.M., Macêdo, P.T., Leão, A.H., Ribeiro, A.M., Izídio, G.S., and Silva, R.H. (2016). Sex and Estrous Cycle Influence Diazepam Effects on Anxiety and Memory: Possible Role of Progesterone. Prog. Neuropsychopharmacol. Biol. Psychiatry *70*, 68–76.

Swanson, L.W., and Hartman, B.K. (1975). The central adrenergic system. An immunofluorescence study of the location of cell bodies and their efferent connections in the rat utilizing dopamine-B-hydroxylase as a marker. J. Comp. Neurol. *163*, 467–505.

Weihe, E., Depboylu, C., Schütz, B., Schäfer, M.K.-H., and Eiden, L.E. (2006). Three types of tyrosine hydroxylase-positive CNS neurons distinguished by dopa decarboxylase and VMAT2 co-expression. Cell. Mol. Neurobiol. *26*, 659–678.

Weirauch, M.T., Yang, A., Albu, M., Cote, A.G., Montenegro-Montero, A., Drewe, P., Najafabadi, H.S., Lambert, S.A., Mann, I., Cook, K., et al. (2014). Determination and Inference of Eukaryotic Transcription Factor Sequence Specificity. Cell *158*, 1431–1443.

Xu, X., Wells, A.B., O'Brien, D.R., Nehorai, A., and Dougherty, J.D. (2014). Cell type-specific expression analysis to identify putative cellular mechanisms for neurogenetic disorders. J. Neurosci. Off. J. Soc. Neurosci. *34*, 1420–1431.